# Integrin-based adhesion compartmentalizes ALK3 of the BMPRII to control cell adhesion and migration

Amaris Guevara-Garcia, Laure Fourel, Ingrid Bourrin-Reynard, Adria Sales, Christiane Oddou, Mylène Pezet, Olivier Rossier, Paul Machillot, Line Chaar, Anne-Pascale Bouin, et al.

# Integrin-based adhesion compartmentalizes ALK3 of the BMPRII to control cell adhesion and migration

Amaris Guevara-Garcia [1, 2, 3], Laure Fourel[1], Ingrid Bourrin-Reynard[1], Adria Sales[2,3], Christiane Oddou[1], Mylène Pezet[1], Olivier Rossier[4], Paul Machillot[2,3], Line Chaar[1], Anne-Pascale Bouin[1], Gregory Giannone[4], Olivier Destaing[1#], Catherine Picart[2, 3#], and Corinne Albiges-Rizo[1*#]

[1] Univ. Grenoble Alpes, Inserm U1209, CNRS 5309, Institute for Advanced Biosciences, Allée des Alpes, Site Santé, F38000 Grenoble, France

[2] Univ. Grenoble Alpes, CEA, Inserm U1292, CNRS EMR BRM 5000, F-38000 Grenoble, France

[3] CNRS, Grenoble Institute of Technology, LMGP, UMR 5628, 3 Parvis Louis Néel, 38016 Grenoble

[4] Univ. Bordeaux, CNRS, Interdisciplinary Institute for Neuroscience, IINS, UMR 5297, F-33000 Bordeaux, France

*To whom correspondence should be addressed

corinne.albiges-rizo@univ-grenoble-alpes.fr

#These authors contributed equally to this work

eTOC: Decoupling of the functions between ALK3 and BMPRII: ALK3 segregation in focal adhesion is BMP2 dependent and BMPRII independent to control cell adhesion processes and SMAD stability.

**Abstract (160 words)**

The spatial organization of cell-surface receptors is fundamental for the coordination of biological responses to physical and biochemical cues of the extracellular matrix. How serine/threonine kinase receptors, ALK3-BMPRII, cooperate with integrins upon BMP2 to drive cell migration is unknown. Whether the dynamics between integrins and BMP receptors intertwine in space and time to guide adhesive processes is yet to be elucidated. We found that BMP2 stimulation controls the spatial organization of BMPRs by segregating ALK3 from BMPRII into β3 integrin-containing focal adhesions. The selective recruitment of ALK3 to focal adhesions requires β3 integrin engagement and ALK3 activation. BMP2 controls the partitioning of immobilized ALK3 within and outside focal adhesions according single-protein tracking and super-resolution imaging. The spatial control of ALK3 in focal adhesions by optogenetics indicates that ALK3 acts as an adhesive receptor by eliciting the cell spreading required for cell migration. ALK3 segregation from BMPRII in integrin-based adhesions is a key aspect of the spatio-temporal control of BMPR signaling.

**Introduction**

The diversity and specificity of cell responses rely on the precise integration of biochemical and physical cues from the microenvironment. Cell-surface receptors and their spatial organization are fundamental for the generation of coordinated responses to the multitude of physical and biochemical cues provided by the extracellular matrix (ECM). ECM proteins can integrate multivalent signals to cells in a spatially patterned and regulated fashion. Fibronectin contributes to concerted cellular responses by providing densely packed binding sites for both adhesive receptor integrins and growth factors and thus potential functional juxtaposition of integrin and growth-factor receptors(Hynes, 2009; Martino et al., 2014). Several studies have reported synergistic effects between integrin mechanoreceptors and growth-factor receptors signaling pathways(Comoglio et al., 2003; Margadant and Sonnenberg, 2010; Ivaska and Heino, 2011). However, the mechanisms and temporal events that enable concerted cellular responses by integrins and growth factor receptors are still unclear.

Integrins are the primary transmembrane receptors that enable cells to respond to external biomechanical cues. We previously found that BMP receptors also directly participate in integrin-mediated force-sensing, as the presentation of BMP2 overrides the effects of soft biomaterial-induced signaling by eliciting a strong biomechanical signaling response(Fourel et al., 2016). When bound to a soft matrix, BMP2 initiates a mechanical response by inducing cell spreading through the formation of β3 integrin-containing adhesion sites and organization of the actin cytoskeleton. In turn, β3 integrin is required to mediate BMP2-induced SMAD signaling. The presentation of BMP2 by the ECM is crucial for optimizing BMP2 signaling through the cooperation between β3 integrin and BMP receptors (BMPRs) to couple cell migration and cell differentiation(Crouzier et al., 2011). However, it is still not known whether such cross-talk involves membrane-proximal interactions between integrins and BMPRs. We also lack information on whether and when these mechanosensitive growth factor receptors and integrins converge at the cell surface.

BMP2 regulates diverse cellular behaviors, ranging from fate specification, lineage selection, and differentiation to epithelial-mesenchymal transition, migration, proliferation, and apoptosis(Nickel and Mueller, 2019). Such diversity of signaling suggests that BMP2 activity is likely dependent both on cell-intrinsic factors, such as the composition of the cell surface

receptor complexes, or the availability of specific transcription factors, and cell-extrinsic factors, such as the activity of other signaling pathways or the physical features of the ECM(Migliorini et al., 2020). BMPRs are present at the cell surface as hetero- or homomeric complexes(Gilboa et al., 2000). BMP2 signaling requires a complex of type-I (e.g., ALK3) and type-II (e.g., BMPRII) serine/threonine kinase receptors to activate the canonical (SMAD) and non-canonical (non-SMAD) signaling pathways upon ligand binding(Nohe et al., 2002; Gilboa et al., 2000). Non-canonical signaling includes several components of other pathways, including MAPKs, ERK1/2, JNK, p38, and Rho-like GTPase(Zhang, 2009; Guo and Wang, 2009). Cell decision-making towards SMAD or non-SMAD signaling may be determined by the lateral mobility of BMPRs. Indeed, ALK3 and BMPRII show distinct lateral mobility within the plasma membrane, which may be required for their involvement in various signaling pathways(Guzman et al., 2012). The ability of ALK3 and BMPRII to have both common and distinct roles correlates with differences in their membrane mobility, which depends on BMP2 binding. However, how canonical and non-canonical BMP signaling are regulated and whether such signaling pathways depend on the specificity of each BMPR subunit remain poorly understood(Li et al., 2017; Nohe et al., 2002). A prerequisite for SMAD-independent signaling is the presence of ALK3 in cholesterol-rich microdomains, which control the lateral mobility of ALK3. This is crucial for regulating non-canonical BMP signaling without affecting canonical signaling(Hartung et al., 2006; Nohe et al., 2002). These studies all suggest that the location of BMPRs relative to their ligands and other receptors is a key aspect of the spatio-temporal control of their complex and multi-decisional signaling.

However, very little is known about whether the spatial arrangement of BMPR affects cellular responses. Whether the dynamics between integrin and BMP receptors is controlled in space and time to guide pivotal intracellular processes is yet to be elucidated. We developed optogenetic tools, including a fluorescent tag, to control and monitor the spatio-temporal dynamics of BMPRs to elucidate whether BMPRs and β3 integrins converge at the cell membrane upon BMP2 stimulation. We found that BMP2 stimulation controls the spatial organization of BMPRs by segregating ALK3 into β3 integrin-containing focal adhesions (FAs), essentially excluding BMPRII. We identified two populations of ALK3 with distinct lateral mobility. The confined population of ALK3 at FAs showed lower mobility than the freely diffusive receptor population far from adhesion sites. The partitioning of ALK3 within FAs

depends on the engagement of β3 integrin with the ECM and is important for modulating β3 integrin clustering, cell spreading, and cell migration.

## Results

### 1. Spatial segregation of ALK3 from BMPRII in focal adhesions upon BMP2 treatment

We previously showed that BMPRs and β3 integrin cooperate to control pSMAD 1/5 signaling upon BMP2 treatment(Fourel et al., 2016). However, little is known about the spatial distribution of BMPRs at the cell surface. As BMP2 signaling can be cell context-dependent, we selected mesenchymal (C2C12, MEFsv40, REF52) and epithelial (Eph4) cell lines and assessed the phosphorylation of SMAD 1/5 following treatment with soluble BMP2 (sBMP2) by western blotting and immunofluorescence **(Supplementary Fig. S1A and S1B)**. Next, we addressed the question of whether growth factor receptors and integrins converge at the cell surface (**Fig. 1A**). We thus designed optogenetic tools to investigate the spatio-temporal control of BMPRs in relation to integrins (**Fig. 1A**). These tools included human ALK3, BMPRII, or CAAX (membrane control) fused to tagRFP-SspB and β3 integrin fused to Venus-iLID (improved light inducer dimer). This optogenetic approach is based on the Venus-iLID micro-system(Guntas et al., 2015), which was developed based on a reversible and light-controlled interaction between two distinct proteins, the bacterial SsrA peptide embedded in the C-terminal helix of a naturally occurring photoswitch, the light-oxygen-voltage 2 (LOV2) domain of *Avena sativa*. We refer to these optogenetic tools as opto-CAAX, opto-ALK3, opto-BMPRII, and opto-β3 integrin. All the opto-constructs were transduced into distinct mesenchymal and epithelial cell lines using lentiviral infection and the populations enriched to obtain a similar level of receptor expression by fluorescence-activated cell sorting (FACS). The exogenous proteins were expressed at the expected molecular weight, as shown by western blotting **(Supplementary Fig. S1C).** We first evaluated the localization of the fluorescently-tagged BMPRs in the dark (i.e., no activation of the photoswitchable domains). Opto-ALK3- and opto-BMPRII showed punctate staining by epifluorescence or confocal microscopy without providing structural information about the membrane **(Supplementary Fig. S1D).** The use of total internal reflection microscopy (TIRFM) improved visualization of these transmembrane proteins through imaging of a thin section of the sample at the interface between the cells and the surface of the glass. We thus observed expression of opto-ALK3 and opto-BMPRII at the cell membrane, whereas opto-β3 integrin was localized to FA sites **(Supplementary Fig. S1D)**. More importantly, TIRFM showed that opto-ALK3 and opto-BMPRII segregate into distinct domains after treatment with soluble sBMP2 in MEFsv40 cells **(Fig. 1B and 1C)**. Indeed, in the absence of BMP2, BMPRs were

distributed throughout the cell surface **(Fig. 1B)**. Upon sBMP2 treatment, opto-ALK3 accumulated in FAs (Fig.1C-D), whereas BMPRII remained excluded **(Fig. 1C-D)**. The localization of opto-β3 integrin was not affected by treatment with sBMP2 **(Fig. 1B-C).** We observed similar spatial segregation between opto-ALK3 and opto-BMPRII upon BMP2 treatment in other mesenchymal cell lines (C2C12 and REF52 cells) **(Supplementary Fig. S2A and 2B).** BMP2 signals through complexes comprising ALK3 with BMPRII or Activin receptor (ACVRIIa/b). However, the segregation of ALK3 into adhesion sites was maintained upon BMP2 treatment even in MEF cells deleted of BMPRII or ActRII by using SiRNA strategy (**Fig. S2C**). This ruled out the possibility for ALK3 to be recruited into FAs under different forms of heterodimers. We could even notice the increase of ALK3 recruitment in FA after deletion of BMPRII, suggesting a role for buffering ALK3 **(Fig. S2C)**. As ALK3 was recruited without BMPRII or ActRII, we addressed the question whether ALK3 could bind BMP2 independently of BMPR to drive adhesive functions. For this purpose, we studied the direct interaction of BMP2 with ALK3 or BMPRII or ActRII by using biolayer interferometry to perform parallel real-time biosensing and to deduce the kinetic parameters (ka, kd) and the equilibrium constant (KD)(Khodr et al., 2021). Our results showed that BMP2 bound to ALK3 with higher affinity than BMPR2, ActRIIA or ActRIIB and that the binding of ALK3 to BMP2 was possible without the need for an oligomerization with BMPR2 or ActRII **(Fig. S3A-E).**

Given that ALK3 localization in FAs is independent of its interaction with BMPRII or ActRIIA/B, our results demonstrate novel spatial segregation of ALK3 and BMPRII, with the accumulation of ALK3 within FAs upon sBMP2 treatment. This suggests that BMPR localization, and consequently BMPR signaling, is spatially regulated, through a specific BMP2 dependent- and BMPRII independent- functionality of ALK3 in FAs.

## 2. Segregation of ALK3 within focal adhesions upon BMP2 treatment depends on β3 integrin engagement

Fibronectin can bind to BMP2 through the FN 12-14 domain, which is close to the FN 7-11 domain, known to mediate its interaction with integrins(Martino et al., 2014). Hence, integrins and BMPRs may be in close functional proximity. Moreover, we previously showed the requirement of fibronectin for cell spreading on bound-BMP2 (bBMP2)-soft matrix through the formation of β3 integrin-containing FAs connected with actin cytoskeleton(Fourel et al., 2016). As fibronectin and vitronectin are both ligands for β3

integrins, we assessed whether vitronectin, like fibronectin(Fourel et al., 2016), may bind BMP2. An ELISA-based solid-phase binding assay showed that there is a direct interaction between BMP2 and vitronectin, in a dose-dependent manner **(Fig. S3F)**. Next, we sought to determine whether β3 integrin engagement can affect the spatial organization of ALK3 and BMPRII. Thus, MEFsv40 co-expressing opto-BMPRs and opto-β3 integrin were plated for 4 h, in the dark, on fibronectin (FN) or vitronectin (VTN)-coated slides, as β3 integrin ligands, or on poly-l-lysine (PLL), as a control of integrin-independent cell adhesion. As expected, cell spreading onto PLL did not induce mature FA formation **(Fig. 2A)**. TIRFM showed punctate staining of opto-ALK3 and opto-BMPRII at the cell surface when the cells were plated on PLL and sBMP2 stimulation did not induce specific BMPR recruitment. The recruitment of opto-ALK3 to FAs only occurred upon sBMP2 treatment of cells plated on vitronectin (VTN) **(Fig. 2B)** or fibronectin (FN) **(Fig. 2C),** which engage β3 integrin to form FAs. Mander's Coefficient was used to quantify the colocalization index between the opto-BMPRs and opto-β3 integrin to assess the proportion of BMPR signal coincident with that of the β3 integrin channel over its total intensity. Higher values indicate greater colocalization. The targeting of opto-ALK3 to β3 integrin-containing FAs was confirmed by a statistically significant increase in the colocalization index of opto-ALK3 on VTN and FN upon sBMP2 stimulation **(Fig. 2D).** By contrast, opto-BMPRII remained distributed throughout the membrane without particular accumulation in adhesion sites, as reflected by cell imaging and the unchanged colocalization index after sBMP2 treatment. Therefore, the partitioning of opto-ALK3 to sites of adhesion is dependent on the presence of extracellular matrix proteins, integrin activation and BMP2, whereas opto-BMPRII remained largely excluded under the same conditions.

As BMP2 induces the tetrameric BMPR complex through the activation of ALK3 by BMPRII(Nohe et al., 2002), we assessed the effect of both a constitutively activated form of ALK3 (ALK3Ca Q233D) and a constitutively inactive form (ALK3Ci, K261R) on the recruitment of ALK3 to adhesion sites. The ALK3Ca receptor harbors a Q to D point mutation at amino-acid 233 in the GS domain, thus replacing activation by BMPRII-mediated phosphorylation in response to BMP ligand binding(Hoodless et al., 1996; Wieser et al., 1995). MEFsv40 cells co-expressing the mutated forms of opto-ALK3 and opto-β3 integrin were allowed to spread on poly-L-Lysine, fibronectin, and vitronectin matrices for 4 h **(Fig.3).** Opto-ALK3Ca was clearly more strongly localized to adhesion sites in cells spread on VTN **(Fig.3B**) and FN **(Fig. 3C),**

independently of sBMP2 stimulation, than on PLL **(Fig. 3A).** Additionally, sBMP2 increased the recruitment of opto-ALK3 and opto-ALK3Ca to adhesion sites in cells spread on VTN and FN but not PLL, as shown by the colocalization index **(Fig. 3D)**. We observed only a slight increase in the colocalization index for opto-ALK3Ci in cells spread on FN upon sBMP2 treatment, likely due to the ability of opto-ALK3Ci to form homodimers with endogenous ALK3. Of note, cells overexpressing opto-ALK3Ca were able to form FAs, even when spread on PLL **(Fig. 3A and E).** This result suggests that the activation of ALK3 is sufficient to promote the formation of adhesion sites and its recruitment. This also supports the notion that type-I receptors may elicit divergent biological responses by signaling to distinct and specific downstream pathways. In conclusion, the microdomain clustering of ALK3 with β3 integrins is highly regulated by both BMP2 stimulation and β3 integrin engagement, suggesting that the spatial control of ALK3 may have specific functional implications for mechanotransduction, cell adhesion processes, or BMP signaling.

### 3. Optogenetic control mimics BMP2 stimulation by targeting ALK3, but not BMPRII, to focal adhesions

We next investigated BMPR segregation and its impact on cell signaling using the second functionality of our BMPR probes allowing an optogenetic approach to control the interaction between BMPRs and β3 integrin. We took advantage of the chimeric receptors in which the iLID (LOV2-SsrA) domain is linked to the intracellular domain of β3 integrin and the SspB peptide fused to the intracellular catalytic domain of each chain of the BMPRs. Upon activation with blue light, the C-terminal helix of the LOV2 domain undocks the protein, allowing the SsrA peptide to bind to SspB **(Fig.1A**).

As previously shown, opto-BMPRs were expressed throughout the cell surface in the dark **(Fig. 4A)**. We assessed the recruitment of opto-CAAX, opto-ALK3, opto-BMPRII, opto-ALK3Ca, and opto-ALK3Ci to FAs containing β3 integrin under the condition of constant pulses of blue light stimulation. All forms of opto-ALK3 and opto-CAAX were recruited to the β3 integrin-FAs, except opto-BMPRII **(Fig. 4B and Video 1-5)**. Clearly, even under conditions of light-induced recruitment of BMPRs to β3 integrin, BMPRII remained excluded from the FAs.

We plotted the normalized intensity of the BMPR signal in the FAs during a time course of light stimulation for multiple cells. The intensity reached a plateau at approximately 180 s of

stimulation for WT ALK3, ALK3Ca, and ALK3Ci (**Fig. 4C**). The patterned recruitment of opto-BMPRs shows the tight spatial and temporal control that the iLID system offers. The observed intensities, as an indication of recruitment, suggest that opto-ALK3Ca had the highest affinity for β3 integrin, whereas it was lower for opto-ALK3Ci and opto-CAAX (**Fig. 4C**), correlating with the sequestration of ALK3 in the FAs induced by sBMP2 **(Fig. 1B**). Such BMPR segregation can be extended to other cell types, since we found that various mesenchymal and epithelial cells, including C2C12, MEFsv40, REF52, and Eph4 cells, showed similar opto-ALK3 recruitment to β3 integrin-containing FAs **(Supplementary Fig. S4 and Video 6-9)**. By contrast, BMPRII remained excluded from FAs, even under blue-light stimulation.

Thus, our date show that the optogenetics approach mimics BMP2 stimulation, as opto-ALK3, but not opto-BMPRII, was targeted to opto-β3 integrin-containing FAs, offering the opportunity to induce rapid and local signal activation. This approach allows us to apply or withdraw the light signal to induce the proximity between ALK3 and β3 integrin. BMPR under optical control provides a powerful approach to actuate and understand ALK3/β3 integrin proximity.

**4. BMP2 treatment leads to decreased ALK3 lateral mobility through its targeting to β3 integrin-containing focal adhesions**

The localization of BMP receptors in distinct plasma membrane domains has been shown to have a major impact on signaling specificity(Guzman et al., 2012). Moreover, varying binding affinities of BMP ligands to type-I and -II receptors contribute to signaling outcomes by creating a preference for a particular receptor subset. We questioned whether BMP2 and, consequently, the targeting of ALK3 to β3 integrin-containing FAs affects the dynamics of ALK3 within the membrane. Thus, we investigated the lateral mobility of BMPRs in living cells using fluorescence recovery after photobleaching (FRAP). FRAP studies were performed on REF52 cells expressing opto-ALK3/β3 integrin or opto-BMPRII/β3 integrin in which we followed the fluorescence recovery of tag-RFP by bleaching a circular region of interest (ROI) overlapping the adhesion sites **(Fig. 5A)**. FRAP was then analyzed by a single exponential fitting equation, with bleaching and background correction, giving the mobile fraction and the characteristic recovery time. At the basal level (unstimulated), the mobile fraction of opto-CAAX was 0.83 ± 0.07 and that of opto-ALK3 0.75 ± 0.13, whereas the mobile fraction

of opto-BMPRII was 0.71 ± 0.13 **(Fig. 5B).** The characteristic recovery time (1/τ) was also extracted from the single exponential fitting curves. A shorter characteristic recovery time indicates faster dynamics and distinct lateral velocities. Opto-CAAX showed faster turnover (13.39 ± 2.53 s), while the turnover of opto-ALK3 and opto-BMPRII was slower (23.57 ± 6.47 and 29.26 ± 6.72 s, respectively). sBMP2 treatment resulted in an increase in the immobile fraction for ALK3, which partially reflects complex formation between ALK3 and BMPRII, as already described(Gilboa et al., 2000; Nohe et al., 2002). After sBMP2 treatment, the mean mobile fraction of opto-ALK3 and opto-BMPRII were not significantly different (0.62 ± 0.25 and 0.63 ± 0.09, respectively). However, we observed a greater standard deviation for the mobile fraction of opto-ALK3, suggesting a heterogeneity in term of molecular dynamics within ALK3 population. Additionally, the presence of sBMP2 increased the time of recovery of opto-ALK3 to 35.42 ± 14.38 s. By contrast, the dynamics of opto-CAAX and opto-BMPRII remained unchanged. We obtained similar results with blue light stimulation instead of sBMP2 **(Fig. 5B and 5C),** indicating that ALK3 becomes immobilized within seconds after ligand addition or light stimulation. Having shown the ability of ALK3 to be recruited to FAs, we assessed the opto-ALK3 mobility outside and within FAs containing β3 integrins by delimiting the ROI. Although, the mobility of opto-BMPRII or opto-CAXX within or outside FAs was not affected by sBMP2, the mobility of opto-ALK3 was reduced within FAs upon sBMP2 treatment, with no significant effects outside of the FAs, suggesting that there are at least two ALK3 populations in term of lateral diffusion **(Fig. 5D)**. FRAP analysis shows the recovery of fluorescence for ALK3 and BMPRII to occur within a time scale of seconds, highlighting the rapid exchange between the receptors at the membrane level. It also shows that a significant portion of ALK3 becomes incorporated into more highly stable complexes with β3 integrin at the cell surface following BMP2 ligand stimulation.

We next used single-protein tracking (SPT) coupled to photoactivation localization microscopy (sptPALM)(Rossier et al., 2012; Chazeau et al., 2014; Manley et al., 2008; Mehidi et al., 2017) to better determine how BMP2 treatment affects the molecular dynamics of ALK3 within and outside β3 integrin-containing FAs **(Fig. 6).** Indeed, SPT could reveal transient immobilization that is concealed within the immobile fractions measured by FRAP(Leduc et al., 2013; Rossier et al., 2012). We analyzed β3 integrin-containing FAs of mouse embryonic fibroblasts (MEFs)(Rossier et al., 2012; Orré et al., 2021) co-transfected

with mEos2-tagged ALK3 proteins and β3-integrin-GFP, as a FA reporter. We acquired high-frequency sptPALM sequences of mEos2-tagged ALK3 (50 Hz, 80s) in between β3-integrin-GFP images to characterize the diffusion of ALK3 within and outside FAs. We reconstructed and analyzed thousands of mEos2-fused protein trajectories, sorted between inside versus outside FAs. After computation of the mean squared displacement, which describes the diffusive properties of a molecule, diffusion coefficients (D) were calculated and the trajectories classified according to their diffusion modes (immobile, confined, free-diffusive) (**Fig. 6A, C, D, E**, see methods)(Rossier et al., 2012; Chazeau et al., 2014). mEos2-ALK3 exhibited free diffusion both within and outside FAs **(Fig. 6A, C, D, E)**. Outside FAs, the fraction of freely diffusing molecules **(Fig. 6D)** increased, at the expense of immobilization, and their rate of free diffusion increased **(Fig. 6E),** indicating that ALK3 diffusion within FAs is slower than outside, most likely due to crowding, as shown for a control trans-membrane protein(Rossier et al., 2012). Super-resolution intensity images showed the selective immobilization of mEos2-ALK3 inside FAs **(Fig. 6A),** explaining the increased immobilized fraction and decreased fraction of freely diffusing molecules found at this location **(Fig. 6C, D)**. Treatment of MEFs with sBMP2 resulted in an increase in ALK3 immobilization both inside and outside the FAs **(Fig. 6B)**. The increase in immobilization was 2.7-fold within FAs (25% to 67%) and 3.4-fold outside (12% to 40%). Moreover, sBMP2 slowed the rate of free diffusion inside and outside the FAs **(Fig. 6E)**. Overall, sBMP2 treatment increased ALK3 enrichment inside the FAs **(Fig. 6F)**. Thus, our results show that sBMP2 treatment induces ALK3 immobilization by a membrane diffusion-trapping mechanism within FAs but also outside. The observed increased ALK3 immobilization outside FAs upon sBMP2 treatment could not be detected in the ensemble FRAP experiments. Thus, the decrease in overall lateral mobility of ALK3 upon BMP2 treatment results from its trapping within FAs, in addition to its well-known association with BMPRII outside FAs.

### 5. Involvement of ALK3 in cell adhesion and migration

Although cells are known to poorly spread over a soft matrix, we have previously shown the involvement of β3 integrin in C2C12 cell spreading and migration induced by soft matrix-bound BMP2(Fourel et al., 2016). We wished to know whether the targeting of ALK3 to β3 integrin-containing FAs upon BMP2 treatment is responsible for such an adhesive process. First, we analyzed the contribution of ALK3 to cell spreading on soft film with matrix-bound

BMP2 (bBMP2). The treatment of C2C12 cells with SiRNA against ALK3 induced cell rounding, indicating a major role of ALK3 in initiation of cell spreading triggered by the presentation of BMP2 by a soft biomaterial. In contrast, the deletion of BMPRII by SiRNA did not affect cell spreading **(Fig. 7A**). However cell spreading was affected by deletion of Src and ILK **(Fig. S5A)** confirming the role of integrin signaling pathway in the BMP2-triggered cell spreading, as previously shown by pharmacological approach(Fourel et al., 2016). Deletion of the tyrosine kinase, FAK, showed no effect on cell spreading, consistent with its role of mechanotransducer in stiffer environment(Zhou et al., 2021). Of note, the deletion of ALK3 also impaired cell spreading in a stiffer environment, when they were spread on FN or VTN-coated glass coverslips **(Supplementary Fig. S5B-C)**. Indeed, cell area **(Supplementary Fig. S5B)** and FA area **(Supplementary Fig. S5C)** were significantly reduced by Si ALK3 treatment but not Si BMPRII treatment. Moreover, cell-tracking assays over 15 h confirmed the ability of bBMP2 to increase migration of cells plated on a soft matrix (velocity of 6 and 42 μm/h, respectively). We previously showed the involvement of β3 integrin in the migration of C2C12 cells seeded onto a BMP2-presenting soft biomaterial(Fourel et al., 2016). We thus addressed whether ALK3 and BMPRII play different roles in cellular migratory behavior. Indeed, only ALK3, but not BMPRII, appears to be involved in cell migration, as the speed of migration was decreased by about two-fold more by ALK3 deletion than by that of BMPRII **(Fig.7B).**

Having shown that ALK3 can be recruited to β3 integrin-containing FAs using optogenetics, we evaluated whether the proximity between ALK3 and β3 integrin affects cell spreading. First, MEFsv40 cells co-expressing opto-CAAX/β3, opto-ALK3/β3, or opto-BMPRII/β3 were spread onto a soft biomaterial presenting or not bBMP2. As previously described(Fourel et al., 2016; Crouzier et al., 2011), all cells displayed a round morphology when seeded on the soft biomaterial alone **(Fig. 7C**), whereas the presentation of bBMP2 by the soft biomaterial was sufficient to permit cell spreading in the dark, regardless of the type of opto-BMPR or opto-CAAX expressed **(Fig. 7D)**. By contrast, upon light stimulation and without BMP2, opto-ALK3/β3 integrin cells were able to spread, while opto-CAAX/β3 integrin cells remained unaffected, revealing the biological relevance of ALK3/β3 integrin proximity in the adhesive cell behavior **(Fig. 7C-D)**. However, the blue-light induction of proximity between opto-BMPRII and β3 integrin also resulted in changes in cell shape relative to opto-CAAX/β3

integrin. To go further, we addressed the question whether FA components, already reported as important for BMP2 signaling, would interfere with ALK3 recruitment upon BMP2 stimulation. Whereas deletion of actors involved in early steps of integrin signaling such as Src and FAK did not perturb the level of ALK3 recruitment in FA, the deletion of ILK, well-acknowledged for ensuring the link between integrins and actin, significantly increased ALK3 recruitment in FA (**Fig. S5D**).

Overall, our results suggest decoupling of the functions between ALK3 and BMPRII in the process of cell adhesion, which is supported by the absence of BMPRII in FAs. Whereas BMP2-induced cell spreading is dependent on ALK3, ALK3 recruitment in FA is regulated by cellular tension controlled by ILK, a downstream effector of β3 integrin.

**6. ALK3 recruitment to focal adhesions is associated with the optimization of SMAD signaling.**

We next studied whether ALK3 recruitment into FAs is associated with SMAD 1/5 signaling. Opto-BMPRs under optical control provide a powerful approach to activate cellular signals and manipulate cell behavior. We thus addressed the question of whether opto-ALK3/β3 integrin proximity leads to BMP2-induced signaling. MEFsv40 cells co-expressing either opto-CAAX/β3 integrin, opto-ALK3/β3 integrin, or opto-BMPRII/β3 integrin were spread onto a soft biomaterial, treated or not with sBMP2, and subjected or not to blue light stimulation. Then, immunostaining against phosphorylated SMAD 1/5 (pSMAD 1/5) was performed before imaging its nuclear translocation **(Fig. 8A and 8B).** Neither overexpression nor the proximity between the opto-BMPRs and β3 integrin could induce the translocation of pSMAD 1/5 in the nucleus in the absence of treatment with BMP2. This is consistent with the requirement of ALK3/ BMPRII heterodimerization to phosphorylate SMAD after activation of ALK3 by BMPRII as already extensively described in the literature(Yadin et al., 2016). However, light stimulation resulted in an increase in nuclear localization of pSMAD solely in the presence of sBMP2 and only following the induction of proximity between ALK3 and β3 integrin (**Fig. 8C and 8D**). P-Smad signal heterogeneity is likely due to different expression levels of integrin and BMPR receptors in between cells. As the proximity between ALK3 and β3 integrin was enough to trigger cell spreading on soft biomaterial devoid of BMP2 **(Fig. 7C-D)**, we investigated whether the cell area might control P-SMAD. We showed that there was no correlation between cell area and P-SMAD **(Fig. S5E)**. We thus hypothesized that the

optimization of P-SMAD signal might result from a defect of SMAD degradation due to a loss of GSK3 activity, since we previously evidenced a role of GSK3 in the BMP-2 mediated cell response(Fourel et al., 2016). Indeed, after phosphorylation of SMAD at the C-terminus by ALK3, the duration of P-SMAD signal is controlled by GSK3-mediated phosphorylation that is required for SMAD1 proteasomal degradation(Fuentealba et al., 2007; Aragón et al., 2011). GSK3 is negatively regulated by ILK, a downstream effector of β3 integrins(Delcommenne et al., 1998) and we have previously shown that β3 integrin is crucial for stabilizing P-SMAD1 by repressing the activity of GSK3 through ILK(Fourel et al., 2016). So, we studied whether ALK3 was more prone than BMPRII to control GSK3 activity. While deletion of ALK3 induces the loss of P-GSK3, deletion of BMPRII led to an increase of P-GSK3 (**Fig S5F**). This is consistent with increase of ALK3 recruitment in FA with β3 integrin when BMPRII is deleted **(Fig. S2C)**. ALK3 population localized with integrins in FA is important to control SMAD degradation in a BMPRII-independent manner. This is consistent with the optimization of SMAD signaling resulting from the light-triggered proximity between ALK3 and β3 integrin **(Fig. 8C and 8D)**. Finally, SMAD signaling is controlled by two populations of ALK3: (i) one combined with BMPR2, outside FA, to control P-SMAD at C-terminus, and (ii) one combined with β3 integrins, within FA to control SMAD stability. These data also evidenced the importance of the temporal dynamics between ALK3 and β3 integrin for optimization of the downstream BMP2 signaling pathway.

**Discussion**

Similar to transforming growth factor-β receptors (TGF-βRs), BMPRs are regulated by the formation of complexes between numerous receptors and co-receptors(Sánchez-Duffhues et al., 2015). Although crosstalk between receptor tyrosine kinase and integrin pathways has been long known(Margadant and Sonnenberg, 2010; Ivaska and Heino, 2011), it has been generally attributed to effects well downstream from the receptors themselves. Very little is known about the control of the spatial arrangement of BMPR subunits and whether their spatial arrangement affects cellular responses to receptor signaling. We previously reported cooperation between β3 integrin and BMPRs to couple cell migration and BMP2 signaling(Fourel et al., 2016). Although the role of β3 integrin was clearly identified in downstream BMP2 signaling(Fourel et al., 2016), information about the events between BMPR subunits and integrins occurring at the cell membrane was missing, partially due to a lack of appropriate tools to monitor BMPR subunit dynamics.

With the design and use of fluorescent optogenetic tools, we demonstrated the novel spatiotemporal regulation of BMPRs and the exclusive participation of ALK3 in the arrangement of FAs and adhesive processes. Indeed, BMPRII is segregated from ALK3 and β3 integrins, which are both localized to adhesion upon BMP2 stimulation. We show that ALK3/BMPRII segregation and exclusive ALK3 enrichment within FAs requires the engagement of both BMP2 and β3 integrin to the extracellular matrix, indicating a very dynamic receptor-ligand relationship. In addition, our dynamic studies based on FRAP and SPT approaches show that BMP2 treatment slows the rate of free diffusion of ALK3 within and outside FAs and increases ALK3 immobilization (**Fig. 6B**), both within (2.7x) and outside (3.4x) FAs **(Fig. 6E)**. Different populations of BMPRs were clearly identified, with distinct lateral mobility. Upon BMP2 treatment, ALK3 receptors partitioned into different domains on the cell surface, corresponding to at least two confined populations of ALK3, one immobilized homogeneously in the plasma membrane, likely through its association with BMPRII, and the other confined to discrete regions, namely FAs, where BMPRII subunits showed no tendency to cluster **(Fig. 9)**. Of note, the partitioning of ALK3 in FA was increased when BMPR2 was deleted suggesting ALK3 buffering by BMPR2. ALK3 recruitment in FA is also tension sensitive since the deletion of ILK showed an increase of ALK3 recruitment in FA **(Fig. S5D)**. Acto-myosin relaxation seems to be required to better integrate Alk3 in FA since

ILK ensures linkage between integrins and the actin cytoskeleton (Stanchi et al., 2009; Sakai et al., 2003) and is a prerequisite for cellular force generation(Martin et al., 2022) by triggering F-actin bundling(Vaynberg et al., 2018). This type of segregation is not restricted to BMPRs and is reminiscent of the differential distribution of TGFβR-I and TGFβR-II in FAs upon TGF-β treatment(Rys et al., 2015). Our results suggest a mechanism driven by the ALK3 cytoplasmic tail for the generation of larger ALK3 clusters to amplify integrin-mediated responses. Indeed, the constitutively active form of ALK3 (ALK3Ca), which harbors the Q233D mutation in the GS domain, was recruited to FAs independently of BMP2 stimulation. This mutation leads to SMAD phosphorylation. However, it may also promote a conformational change in the intracellular domain of ALK3 to expose sites of phosphorylation or provide a docking site for specific kinases or signaling molecules to control both ALK3 recruitment and the regulation of adhesion sites.

How these larger-scale domains are built from ALK3 nanoclusters is unknown and is a subject for further investigation. We previously showed the requirement of fibronectin in cell spreading induced by BMP2(Fourel et al., 2016). Our results showing higher affinity of ALK3 for BMP2 independently on its interaction with BMPRII **(Fig. S3**) support ALK3 recruitment in FA (Fig. 1, 2, 5, 6) independently of its interaction with BMPR2 (**Fig. S2C**). Our data are consistent with the BMP2 dependent- and BMPRII independent- functionality of ALK3 in FAs. A physical mechanism may be provided by the close proximity between the integrin-binding and BMP2-binding domains of Fibronectin(Martino et al., 2014; Hynes, 2009) **(Fig. 9)**. It is yet to be determined why ALK3 is more readily recruited to FAs than BMPRII upon BMP2 treatment. It has been reported that many of the molecular components that regulate cell-ECM adhesion are associated with cholesterol and sphingolipid-enriched detergent-resistant membrane (DRM) microdomains, which are also enriched in the acidic phospholipid PI(4,5)P2 (Pande, 2000; Márquez and Sterin-Speziale, 2008). Lipid modifications, such as palmitoylation, enable molecules to partition into such locally generated specific microenvironments(Lorent and Levental, 2015; Lorent et al., 2017). The ability of ALK3 to mainly associate with DRM fractions, likely through its being S-acylated(Wegleiter et al., 2019), could explain the segregation between ALK3 and BMPRII. Whether ALK3/β3 integrin receptor clusters are formed through the physical process of

'phase separation' to build molecular platforms that drive key cellular functions is yet to be explored(Banjade and Rosen, 2014; Li et al., 2012; Chong and Forman-Kay, 2016).

The segregation between ALK3 and BMPRII may also constitute the mechanosensitive control of ALK3/BMPRII multimerization and function depending on the level of BMP ligand stimulation. The various modes of BMPR oligomerization, such as ALK3 homodimerization and ALK3/BMPRII tetramerization, might dictate the specificity of downstream signaling pathways and transcriptional responses. Indeed, ALK3 and BMPRII show distinct lateral mobility within the plasma membrane in response to BMP2, which is required for their involvement in various signaling pathways(Guzman et al., 2012; Gilboa et al., 2000). Such shifting may depend on the specificity of ALK3 and BMPRII to associate with different co-receptors. Our study highlights the ability of ALK3, but not BMPRII, to segregate with β3 integrin within mature FAs. The reduced lateral mobility and accumulation of ALK3 receptors in microdomains, such as FAs, at the cell membrane is associated with adhesion and migration. The biological relevance of such proximity between ALK3 and β3 integrin is underlined by the cells' ability to spread onto a soft matrix and optimize SMAD 1/5 signaling using optogenetic tools. Whereas cell spreading mediated by integrin is clearly initiated by BMP2 and ALK3 recruitment in FA, there is no correlation between cell area and Smad signaling **(Fig. S5E)**. The optimization of SMAD signaling resulting from the recruitment of ALK3 in FA by optogenetics **(Fig. 8C-D)** is on line with the previously established role of β3 integrin in controlling Smad turnover through GSK3 activity(Fourel et al., 2016). Here we confirm that ALK3 similarly to β3 integrin is more efficient than BMPRII in controlling GSK3 activity. This suggests the coupling between ALK3 and β3 integrin to control GSK3 phosphorylation and to limit SMAD degradation **(Fig. 9)**. The spatial organization of ALK3 within FAs also provides a new means for the mechanical control of integrin clustering and FA formation. As already reported(Hiepen et al., 2019), BMPRII may play the role of gatekeeper to limit FA formation and cell spreading, as shown by the ability of cells depleted of BMPRII to spread more and to develop more FAs **(Fig. S5A and Fig. S5B-CA-B)**. These results suggest that ALK3 and BMPRII are involved in the regulation of adhesion by playing opposite roles in the control of FA dynamics.

The partitioning of ALK3 within and outside FAs shows two potentially differentially regulated populations of ALK3 receptors associated either with β3 integrin or BMPRII **(Fig.**

**9)**. This may also contribute to the context-dependent signaling outcomes of the BMP pathway. Indeed, BMP pathway activation depends on environment stiffness(Sales et al., 2022) and on combinatorial interactions between BMPs(Klumpe et al., 2022). Cells may also finely control the functional presentation and activation of heteromeric receptor complexes, and thus, define their context-dependent responsiveness to ligands. As an example, BMP ligand expression is elevated in patients with breast cancer and ALK3 expression has been shown to correlate with a poor prognosis(Owens et al., 2012). Moreover, the attenuation of BMPRII signaling in mammary carcinoma cells enhances metastasis, whereas ALK3 deletion impairs mammary tumor formation and metastasis(Owens et al., 2012, 2014, 2015). Similar to TGF-β, over-expression of BMP2/4 and the alteration of BMPRs have been reported in several cancer tissues, including melanoma and colon, lung, and breast cancer (Przybyla et al., 2016; Rothhammer et al., 2005; Rajski et al., 2015). Given the higher affinity of ALK3 for BMP2(Khodr et al., 2021) , our results may explain the duality between ALK3 and BMPRII in metastasis through the involvement of ALK3 and, to a lesser extent, BMPRII in cell migration in response to BMP2. The accumulation of ALK3Ca in FAs independently of the presence of the BMP2 ligand also provides clues about the adhesive properties of ALK3. The trapping of ALK3 in FAs may be a signature of invasiveness. Consistent with this hypothesis, expression of the constitutively active form of ALK3 induces Id1 protein(Shepherd et al., 2010) and β-catenin expression. Id1 has been shown to contribute to tumorigenesis by inhibiting cell differentiation, stimulating proliferation, and facilitating tumor neoangiogenesis(Perk et al., 2005) and β-catenin has already been described as an EMT marker(Kim et al., 2019). The partitioning of ALK3 between BMPRII and β3 integrin provides a new mechanism to control the diversity of BMP signaling, couple cell functions, such as cell migration and cell differentiation, and participate in pathological processes when dysregulated.

Overall, our data show that the localization of ALK3 relative to other receptors, notably β3 integrin, is a key aspect of BMP2 signaling in cell adhesion and migration. BMPR segregation may be a process to balance SMAD and non-SMAD signaling. The control of cell spreading, cell migration, and cell metastasis might be also considered as a new non-SMAD pathway downstream of BMP2 signaling. BMPR segregation needs to be further studied to have a comprehensive view of ALK3 in physio-pathological situations.

## Materials and Methods

### Preparation of PLL/HA films, cross-linking, and BMP2 loading

HA (sodium hyaluronate, $2x10^5$ g/mol) was purchased from Lifecore Biomedical (USA) and PLL (Poly-L-Lysine, $2x10^4$ g/mol) from Sigma (France). PLL (0.5 mg/mL) and HA (1 mg/mL) were dissolved in Hepes-NaCl buffer (20 mM Hepes pH 7.4, 0.15 M NaCl). PLL/HA films were prepared as previously described(Machillot et al., 2018) in 24- and 96-well plates with an automated film-layering procedure using a liquid handling robot. The films were cross-linked as previously described(Crouzier et al., 2011) using 1-ethyl-3-(3-dimethylamino-propyl) carbodiimide at 30 mg/ml (low-crosslinked (CL), soft films) or 70 mg/ml (high CL, stiff films) and N-hydro-sulfosuccinimide at 11 mg/ml (both purchased from Sigma-Aldrich). BMP2 (clinical grade; Medtronic) was incorporated into the films pre-equilibrated for 30 min in the medium in which BMP2 was suspended (1 mM HCl). BMP2 was deposited onto the films and left to adsorb for 1 h at 30°C. The coated slides were thoroughly washed for 1 h in HEPES-NaCl to retain only the matrix-bound BMP2(Crouzier et al., 2011). Cell spreading and pSMAD1/5/9 immunofluorescence were imaged using a high content imaging system (GE INCA 2500 imaging system, General Electrics Healthcare, France). Automated analysis was then performed using a dedicated software (InCarta software, General Electrics Healthcare, USA) as recently published(Sales et al., 2022) to segment cells and nuclei, and to quantify cell area and pSMAD signal intensity.

### Design of plasmids

All constructs were cloned into the lentiviral backbone, p-lenti, with the CMV promoter to drive β3 integrin expression and Psico, with the mpGK promoter to drive BMP receptor expression. The C-terminus of the opto-fluorescent protein was fused to the receptors of interest. pLL7.0: Venus-iLID-CAAX (from KRas4B) (Addgene plasmid # 60411; http://n2t.net/addgene:60411;RRID: Addgene 60411) and pLL7.0: tgRFPt-SSPB R73Q (Addgene plasmid # 60416; http://n2t.net/addgene:60416;RRID: Addgene_60416) were gifts from Brian Kuhlman. Constitutively inactive ALK3 (ALK3Ci) (K261R) and constitutively active ALK3 (ALK3Ca) (Q233D) were obtained by point mutations and fused to RFPsspB. The engineered primers were designed using the nebbuilder tool (New England Biolabs (NEB)) and synthesized by Eurofins genomics. The constructs were cloned using Phusion high-fidelity DNA polymerase by PCR amplification and subsequent Gibson assembly (NEB).

Screening for the correct plasmid product was carried out by bacterial transformation and restriction-site digestion. The DNA was isolated from the cultures using the Nucleo bond Xtra plasmid DNA purification kit (Machery-Nagel). The constructs were verified by sequencing using the target sequences listed in Supplementary Table S1 (Light run, Eurofins genomics).

**Cell culture, cell transfection, and viral transduction**

MEFsv40 cells (CRL-2907, American Type Culture Collection ATCC), REF52 cells (CVCL_6848), and HEK 293 ft cells were cultured in DMEM medium and C2C12 cells (CRL-1772, American Type Culture Collection (ATCC) in DMEM: Ham's F12 medium (11320, Gibco). The media was supplemented with 10% FBS (FBS, PAA Laboratories) and penicillin-streptomycin. Eph4 cells were cultured in DMEM supplemented with 10% newborn calf serum (Thermo Fischer Scientific, 26010074) and penicillin/streptomycin. Transient transfections were performed using Jet Prime (polypus transfection) or lipofectamine 2000® (Gibco, Invitrogen) following the manufacturer's protocol. All cell types were incubated at 37°C in 5% $CO_2$ in a standard humidified incubator.

Homemade-lentiviruses were produced by co-transfecting HEK293 ft cells with pC57GPBEB GagPol MLV, pSUSVSVG, and the plasmid of interest using lipofectamine2000 (Invitrogen). The viral supernatant was collected and concentrated using LentiX concentrator (Takara réf:631232 Lenti-X Concentrator). Viral production was optimized by the Vectorology platform (SFR BioSciences, UMS3444/US8) and the virus provided following concentration by ultracentrifugation and FACs titration (UI/mL). Cells were infected by directly adding the appropriate volume of concentrated virus supernatant to obtain the optimal multiplicity of infection (MOI).

For SiRNA transfection, cells were seeded at 70% confluency in six-well plates, cultured overnight, and transfected twice at 24-h intervals with 30 nM siRNA (ON-TARGET plus SMARTpool) and Lipofectamine RNAi max (Life Technologies, ref. 13778-150) in Opti-MEM medium (Gibco) according to the manufacturer's instructions at 37°C in a standard 5% $CO_2$ humidified incubator. The level of depletion was analyzed by quantitative PCR. The primers used are listed in Supplementary Table S2. The cells were then detached using trypsin-EDTA and seeded into Lab Tek chambers coated with either fibronectin, vitronectin, or poly-L-Lysine for colocalization studies.

**Flow cytometry (intensity normalization and sorting)**

After reaching 80% confluency, the infected cells were suspended in a small volume of PBS without Ca/Mg (˜200 µl per a 10 cm plate). Cells of interest were selected through fluorescence-activated cell sorting (FACS). The cell suspension was run on an Aria IIu sorter (BD Biosciences) and the cells sorted by BMPR expression based on tagRFP and integrin β3 fluorescence intensities, excited by 561-nm and 488-nm lasers and collected through 610/20 nm and 530/30 nm bandpass filters, respectively. The tagRFP intensity window was selected using $2x10^4$ to $7x10^4$ non-infected (wildtype) compensation control cells to correct for spectral overlap between GFP and tagRFP.

**Total internal reflection imaging**

Cells were imaged using an iMIC2.0 (TILL Photonics) equipped for total internal reflection fluorescence microscopy (TIRFM) and photoactivation (Yanus scan head) with a 63x NA 1.46 plan-apochromatic oil immersion objective (Carl Zeiss). Images were acquired using an iXon U-897 EMCCD camera (Andor) with LA software (TILL Photonics). Cells were maintained at 37°C and 5% $CO_2$ in a stage-top incubator (IBIDI). Lab-Tek coverglass-bottom chambers (Thermo Fisher Scientific) were used for imaging and the media replaced by fluorobrite DMEM (Gibco). A 488-nm excitation laser was used to both observe proteins fused to the Venus fluorescent protein and activate the optogenetic system, thus inducing the interaction of the complement optogenetic protein fused to SspB. A 561-nm excitation laser was used for the observation of proteins fused to RFP without causing activation of the optogenetic system.

**Receptor localization**

Opto-cells were cultured for 4 h in Lab-Tek chambers (Thermo Fisher Scientific) coated with Poly-L-lysine (P9404, Sigma-Aldrich, 10 µg/mL), fibronectin (home-made, 5 µg/mL), or vitronectin (3186, Sigma-Aldrich, 5 µg/mL). Soluble BMP2 (600 ng/mL) was added to half of the samples. The samples were chemically-fixed with 4% paraformaldehyde (PFA) and TIRFM imaging was performed. ImageJ (FIJI) was used for image processing and analysis. Merged channels and plot profiles across all FAs are presented. The image intensity of both channels in the FA region was quantified to provide a measure of correlation using the Manders coefficient calculated by the ImageJ (v1.45d, NIH, Bethesda), plugin JACoP. (Bolte and Cordelières, 2006)

**Optogenetic experiments**

Optogenetic stimulation of BMPRs recruited to FAs includes three steps: i) the capture of a few images every 10 s acquired using a 561-nm laser to ascertain the basal state and position of the BMPRs, ii) multichannel acquisition to activate the optogenetic system using 488-nm and 561-nm lasers every 10 s for 3 min, and, finally, iii) a dissociation step, with images acquired using only the 561-nm laser every 10 for 3 min All images were processed with ImageJ software. BMPR recruitment was quantified over time using the RFP channel of each TIRF image in the regions of interest (ROI) delimitated by the FA using the Time Series Analyzer plugin (RRID:SCR_014269) of Fiji software(Schindelin et al., 2012). Each intensity value was normalized using the intensity at the membrane over time.

Cell population photo-stimulation was performed using a customized blue LED device adapted from the Janovjak Laboratory(Grusch et al., 2014). The device consists of an aluminum box equipped with 300 light-emitting diodes (JS-FS5050RGB-W30 with a JS-CON-004 controller; Komerci, Ebern, Germany) placed in a cell-culture incubator. Light intensity was controlled using an analog dimmer and measured with a digital power meter (SanwaLP1).

For the measurement of the BMPR recruitment within FAs, β3-integrin FAs were used to predefine ROIs. A macro was written in Fiji to semi-automate RFP-intensity measurement inside the ROIs.

**Fluorescent recovery after photobleaching**

Cells were seeded in Lab-Tek coverglass chambers (Thermo Fisher Scientific) overnight at 40% confluency. The media was then replaced by fluorobrite DMEM (Gibco) supplemented with 10% FBS and L-glutamine (1 mM) 2 h prior to experiments. Before starting the FRAP experiments, the media was replaced by low-serum Fluorobrite (0.5% FBS) and images of 10 cells acquired over 1 h. Then, cells were treated with BMP2 (600 ng/mL) or stimulated with blue light for 1 min. Images of 10 cells were acquired over 1 h. A 10-µm diameter ROI was scanned using the 561-nm laser diode (100%, 3 ROI loop count) to bleach the fluorophores. The recovery of fluorescence after photobleaching was followed over time (acquisition every 2 s for 2 min) and corresponds to the arrival of a new pool of molecules in the ROI allowing study of the temporal dynamics of fluorescently-tagged proteins (CAAX, ALK3, BMPRII). The fluorescence of the whole cell was also tracked over time as a control for bleaching.

FRAP analysis was performed using offline analysis software (OA-TILL Photonics) with the offline FRAP tool option. A single exponential model was applied to the fluorescence intensity recorded for the bleached region A*(1-exp[-t*tau_frap]) after normalization against the total cell fluorescence intensity and camera background. The characteristic recovery time (1/τ) of BMPR-RFP from the fit of the experimental data consisted of the mean of the values for at least 20 cells.

**Single-protein tracking by sptPALM acquisition**

MEF cells stably transfected with β3-integrin-GFP were transiently transfected with mEOS2 Alk3. Cells were imaged at 37°C with an iMIC2.0 (TILL Photonics) equipped for total internal reflection fluorescence microscopy (TIRF) microscopy and photoactivation (Yanus scan head) with a 63x NA 1.46 alpha Plan-Apochromat oil immersion objective (Carl Zeiss). Images were acquired using an iXon U-897 EMCCD camera (Andor) with LA software (TILL Photonics). Lab-Tek coverglass-bottom chambers (Thermo Fisher Scientific) were used for imaging and the media was replaced by Ringer's solution. For photo-activation localization microscopy, cells expressing mEOS2-tagged constructs were photo-activated using a 405-nm laser and the resulting photoconverted single-molecule fluorescence signal was excited with a 561-nm laser. The two lasers simultaneously illuminated the sample. Their respective power was adjusted to keep the number of stochastically activated molecules constant and well separated during the acquisition. Acquisition was performed in streaming mode at 50 Hz. Sequences of 16,000 images were acquired for each cell. The 488-nm excitation laser was used to observe β3-integrin-GFP enriched FAs before each tracking.

**sptPALM segmentation and tracking**

A typical sptPALM experiment leads to a set of 16,000 images per cell, which are then analyzed to extract information about the localization and dynamics of the molecule. Single-molecule fluorescent spots were localized and tracked over time using a combination of wavelet segmentation and simulated annealing algorithms developed in Metamorph software (Molecular Devices), as described previously(Chazeau et al., 2014; Mehidi et al., 2017; Rossier et al., 2012). For ALK3 enrichment and trajectory analysis, ROIs of FAs were identified manually from GFP-β3-integrin images. The corresponding binary masks were used to sort single-particle data to specific regions, namely within or outside FAs. ALK3 enrichment in FAs was measured as the ratio of within versus outside detection of

fluorescent events. Furthermore, we analyzed trajectories lasting at least 260 ms (≥ 13 points) using a custom Matlab routine that analyzes the mean squared displacement (MSD), which describes the diffusion properties of a molecule, computed as in (Eq. 1):

$$\mathrm{MSD}(t = n \cdot \Delta t) = \frac{\sum_{i=1}^{N-n}(x_{i+n} - x_i)^2 + (y_{i+n} - y_i)^2}{N - n} \quad \text{Eq. 1}$$

where $x_i$ and $y_i$ are the coordinates of the label position at time $I \times \Delta t$. We defined the measured diffusion coefficient $D$ as the slope of the affine regression line fitted to the $n$ = 1 to 4 values of the MSD($n \times \Delta t$). The MSD was computed and then fitted to a duration equal to 80% (minimum of 10 points, 200 ms) of the whole stretch by (Eq. 2):

$$\mathrm{MSD}(t) = \frac{4r_{\mathrm{conf}}^2}{3}(1 - \mathrm{e}^{-t/\tau}) \quad \text{Eq. 2}$$

where $r_{conf}$ is the measured confinement radius and $\tau$ the time constant $\tau = (r_{conf}^2 / 3D_{conf})$. We used a weighted fit to reduce the inaccuracy of the MSD fit due to down sampling for larger time intervals. Trajectories were sorted into three groups: immobile, confined diffusion, and free-diffusion, as described previously(Mehidi et al., 2017; Chazeau et al., 2014; Rossier et al., 2012). Immobile trajectories were defined as trajectories with D < 0.011 $\mu m^2.s^{-1}$, corresponding to molecules that explored an area inferior to that defined by the image spatial resolution ~(0.05 µm)² during the time used to fit the initial slope of the MSD(Rossier et al., 2012). We used the time constant calculated $\tau$ for each trajectory to separate trajectories displaying free diffusion from those displaying confined diffusion. Confined and free diffusion events were defined as trajectories with a time constant inferior or superior, respectively, to half the time interval used to compute the MSD (100 ms).

**Immunofluorescence**

Cells were seeded on glass coverslips and stimulated with 600 ng/mL BMP2 or constant pulses of blue light illumination for the indicated time (Lab Tek or coverslip). The cells were fixed with 4% PFA for 10 min at room temperature, washed three times with PBS, and permeabilized for 15 min with PBS containing 0.3% Triton X-100 and 0.5% Tween-20 (TBST). Permeabilization was not required the labeling of membrane proteins. After blocking with 4% goat serum in PBS for 1 h, cells were incubated with the primary antibody (α-pSMAD 1/5 (Cell signaling 13820) or β3 integrin (EMFRET, M030-0)) diluted in blocking solution for 2 h.

Samples were then washed, incubated with a secondary Alexa Fluor-conjugated antibody (Thermo Fisher Scientific) for h in 1% bovine serum albumin (BSA)/TBST and Alexa-Fluor 647-phalloidin (A22287), when required, and finally washed and mounted using mowiol-containing DAPI (Santa Cruz). Nuclear translocation of transcription factors was quantified by measuring their mean intensity inside the nucleus, segmented from the DAPI staining.

**Immunoblotting**

Cells were seeded in 6- or 12-well plates overnight. Depending on the experimental conditions, cells were starved for 3 h and stimulated with BMP2 or blue light pulses for the indicated times. Cells were lysed in RIPA buffer (TBS, 50 mM NAF, 40 mM, Nappi, 1% Triton X-100, 0.1% SDS) supplemented with protease and phosphatase inhibitors. Laemmli buffer (2X) was added and the tubes heated to 95°C for 5 min. The lysates were run in 8-10% polyacrylamide gel at 30 mA/gel and transferred onto nitrocellulose or PVDF (polyvinylidene difluoride) membranes using transfer buffer containing 20% isopropanol and 0.04% SDS. After electro-transfer (110v, 1h20), membranes were blocked in TBS-Tween-20 (0.1% v/v) containing low fat milk (5%) at room temperature for 1 h. Then the PVDF membranes were incubated with primary antibodies, diluted to their corresponding final dilution, in TBS-T, containing 5% BSA overnight at 4°C: anti-pSMAD 1/5 (Cell signaling 9516), anti- β3 integrin (Emfret M030-0), anti-tagRFP (Evrogen AB233), anti-GAPDH (GT239, Genetex). After three washes, membranes were incubated with an HRP-conjugated secondary antibody diluted in TBS-Tween-BSA, for 1 h at room temperature. After an additional three washes, peroxidase activity was visualized by chemiluminescence (Enhance Chemi-Luminescence, Thermo Scientific) using the ChemiDoc MP imaging system (Biorad) or a fusion fx camera (Vilber, smart imaging). GAPDH was systematically included as a loading control. The intensity was analyzed using Image J (Fiji).

**Cell spreading**

Cells were seeded onto soft (low-crosslinked) PLL/HA films for 4 h in the presence of bound or soluble BMP2, with or without blue illumination (10 s pulses) for 4 h. The cells were washed with PBS and fixed with PFA 4% for 10 min. After washing with PBS, actin was fluorescently labeled (Alexa Fluor™ 647 Phalloidin). Cells were kept in PBS and image acquisition was performed using an iMIC2.0 (TILL Photonics) inverted microscope in the epifluorescence mode. The data collected was analyzed by ImageJ software (v 1.45p, NIH) to

calculate the area of the cell. Another macro was written for quantification of the cell number and the area of spreading. Images of the nuclei were binarized using an intensity threshold. Touching nuclei were separated using the watershed function.

**Cell migration assay**

To follow cell migration, C2C12 cells were seeded at $15x10^3$ cells/$cm^2$ on high-CL films with bound BMP-2 in 24 well plates. Time-lapse images were acquired every 15 min over a 16-h period (after the initial 4-h adhesion period) using a 10×/0.3 NA objective with a phase-contrast microscope (AxioObserver Z1; ZEISS) equipped with an incubator to maintain the cells at 37°C and 5% $CO_2$. Images were acquired with ZenBlue software using a CoolSNAP HQ2 CCD camera (Roper Scientific). For the analysis, at least 20 cells were tracked using ImageJ (v1.45d, NIH, Bethesda). After cell tracking, the cell paths were plotted using the Chemotaxis and Migration tool (Ibidi), which allows the quantification of cell velocity and directionality.

**Solid Phase-based Binding Assay**

A 96-well plate (R&D System ref. DY990) was coated with 5µg/mL BMP2 (kit Inductos - Medtronic) at pH3 or 5µg/mL BSA (Millipore ref.82-045-1) overnight at room temperature. After three washes in PBS, 0.1% Tween 20, plate was blocked with 5% BSA solution for 2h at room temperature. Increasing concentrations of vitronectin (Sigma ref.90987) were incubated in PBS for 2 h at 37 °C. After three washes in PBS, 0.1% Tween 20, detection of bound vitronectin was performed using successively the mouse monoclonal antibody directed against vitronectin (abcam ab201981) and secondary anti-mouse antibody coupled to HRP. Revelation was done with Peroxydase substrate kit (R&D System ref. DY999) for 20min and reaction stopped with 2M H2SO4, then absorbance was read at 450nm and 620nm. Data shown are the means of duplicate determinations, and error bars represent standard deviations. The figure illustrates one representative experiment of three performed experiments with similar results.

**Biolayer interferometry/BLI kinetics interaction experiments**

All the BLI experiments were performed using an OctetRED96e apparatus from Pall/FortéBio (California, USA) and data were recorded with the manufacturer software (Data Acquisition v11.11). In detail, prior to any capture, the BMPR-Fc samples were first diluted in the HEPES-

NaCl buffer. For the association phase, the BMPs were diluted in two-fold serial dilutions in HEPES-NaCl buffer. 0.2 ml of each sample and buffer were disposed in wells of black 96-well plates (Nunc F96 MicroWell, Thermo Fisher Scientific), maintained at 25°C and agitated at 1000 rpm the whole time. Prior to each assay, all biosensors were prewetted in 0.2 ml of HEPES-buffer for 10 min, followed by monitored equilibration for 60 or 120 s. AHC capture biosensors (FortéBio) were loaded with each ligand for 200 s until reaching a spectrum shift between 0.8 and 1.1 nm depending on BMPR-Fc, followed by an additional equilibration step of 60 or 120 s in HEPES-NaCl buffer. Association phases were monitored during dipping the functionalized biosensors in analyte solutions of different concentrations between 2 and 80 nM for 400 s, and the dissociation phases in the buffer for 400 s. All measurements were performed three times in independent experiments. Kinetics data were analyzed using the manufacturer software (Data analysis HT v11.1). The "blank" signal from the biosensor in the presence of the HEPES-NaCl buffer was subtracted from the signal obtained from each functionalized biosensor and each analyte concentration. The kinetic signals were then fitted using a global/local method and 1:1 Langmuir. Affinity constants were calculated from the ratio kd/ka values. The reported values are given as mean ± SD obtained from three independent experiments.

**Statistical analysis**

Graphical data visualization and statistical analysis were performed using Prism 7 (GraphPad). Statistical comparisons between two samples were performed using the unpaired t-test if the variances were equal. Statistically significant values are reported on the figures according to the p-value.

**Online supplemental material**

**Fig. S1** shows the ability of the selected cell lines to respond to soluble BMP2 and validates the expression of opto-BMPRs and opto-β3 Integrin. **Fig. S2** shows the recruitment of ALK3 in adhesion sites in different cell types without the requirement of BMPRII. **Fig. S3** shows the binding properties of BMP2. **Fig. S4** shows ALK3 targeting in FAs after blue light stimulation in mesenchymal and epithelial cells. **Fig. S5** shows the signaling pathways required for maintaining cell spreading and Smad signaling induced by BMP2. **Video 1** shows the recruitment of CAAX to adhesion sites upon optogenetic control of CAAX/β3 integrin proximity. **Video 2** shows the recruitment of ALK3 to adhesion sites upon optogenetic

control of ALK3/β3 integrin proximity. **Video 3** shows the exclusion of BMPRII from adhesion sites upon optogenetic control of BMPRII/ β3 integrin proximity. **Video 4** shows the recruitment of ALK3Ca to adhesion sites upon optogenetic control of ALK3Ca/β3 integrin proximity. **Video 5** shows the limited recruitment of ALK3Ci to adhesion sites upon optogenetic control of ALK3Ci/β3 integrin proximity. **Video 6** shows the recruitment of ALK3 in β3 integrin-containing FAs in C2C12 cells after light stimulation. **Video 7** shows the recruitment of ALK3 in β3 integrin-containing FAs in MEFsv40 cells after light stimulation. **Video 8** shows the recruitment of ALK3 in β3 integrin-containing FAs in REF52 cells after light stimulation. **Video 9** shows the recruitment of ALK3 in β3 integrin-containing FAs in Eph4 cells after light stimulation. **Table S1** lists primers used for plasmid sequencing. **Table S2** lists primers used for qPCR.

**Acknowledgements:** We thank the staff of the bioimaging facility of the Institute for Advanced Biosciences (MicroCell) for their help with imaging, cell sorting, and analysis. We thank Gisèle Froment, Didier Nègre, and Caroline Costa from the lentivirus production facility / SFR BioSciences Gerland - Lyon Sud (UMS3444/US8). We also thank Agnieszka Kawska (http://www.IlluScientia.com) for the artwork associated with Fig. 9. We thank Valia Khodr for the measurements of BMP2/BMP receptor interactions. AGG was funded by CONACYT (CVU :532484) and the ANR (ANR-17-CE13-022). This research was funded by an ANR grant (ANR-17-CE13-022), an FRM grant (DEQ20170336702), and HTE ITMO CANCER (PITCHER) to C.A-R and by an FRM grant (DEQ20170336746) to C.P. CP is a senior member of Institut Universitaire de France, whose support is greatly acknowledged.

**Authors' contributions**

A. Guevara-Garcia designed and performed most of the experiments and analyzed the data. L. Fourel and C. Albiges-Rizo initiated the project. L. Fourel performed the cell migration assays. L. Fourel and M. Pezet performed the SPT experiments. I. Bourrin-Reynard performed the cell infection and cell sorting. I. Bourrin-Reynard and A.-P. Bouin quantified the cell spreading assays and the level of BMPR recruitment. L. Chaar performed GSK3 and Smad quantification. A. Sales performed the cell-adhesion experiments on the PLL/HA films.

C. Oddou, A. Guevara-Garcia, and L. Fourel designed and constructed the plasmids. C. Picart provided funding for the biomaterials part, designed experiments related to PLL/HA films, and contributed to data analysis. P. Machillot provided the PLL/HA films, performed siRNA experiments on biomaterials and ECM protein binding experiments. G. Giannone and O. Rossier performed the SPT analyses. O. Destaing analyzed the optogenetics and FRAP data. C. Albiges-Rizo conceived and supervised the project, designed the experiments, analyzed the data, and wrote the paper. All authors commented on and edited the manuscript.

The authors declare that they have no competing interests.

## Figure legends

**Figure 1. Spatial organization of ALK3 from BMPRII in focal adhesions.** (A) Schematic of whether cross-talk between integrin and BMPR relies on proximal interaction at the cell membrane (left panel). Fluorescent and optogenetic tools are used to image BMPRs and β3 integrin and to control BMPR/β3 integrin proximity respectively. ALK3 is given as an example of BMPR (right panel). Optogenetic tool (iLID/SspB) allows the blue light-induced intracellular interaction between β3 integrin and ALK3 is shown, as an example. (B) Opto-BMPRs-RFP and opto-β3 integrin-Venus are co-expressed in MEFsv40 and visualized by TIRF-mode imaging. Without BMP2 treatment, BMPRs were localized throughout the cell surface and β3 integrin was targeted to FAs. (C) sBMP2 treatment induces spatial segregation of ALK3 from BMPRII at adhesion sites. Scale bar 15 µm. (D) Quantification of the ratio of the level of recruitment inside and outside focal adhesions, identified by β3 integrin (Venus tag), on cells expressing of ALK3, BMPRII or CAAX (RFP tag) upon BMP2 stimulation. N ≥ 14 cells per condition.

**Figure 2. The spatial organization of ALK3 in adhesion sites upon BMP2 treatment depends on β3 integrin engagement with the extracellular matrix.** Opto-BMPRs-RFP and opto-β3 integrin-Venus were co-expressed in MEFsv40 cells and observed by TIRF-mode imaging. MEFsv40 cells were treated or not with sBMP2 and seeded onto (A) poly-l-lysine (PLL)-coated substrates, facilitating integrin-independent cell adhesion, and onto (B) vitronectin (VTN)- or (C) fibronectin (FN)-coated substrates to engage β3 integrin. Opto-ALK3 recruitment to adhesion sites induced by sBMP2 is dependent on integrin binding to VTN and FN. (D) Quantification of the colocalization index using Manders coefficient shows the recruitment of Opto-ALK3 to FAs upon β3 integrin binding to VTN or FN and the presence of sBMP2. N= 20 cells per condition. Scale bar 15 µm. ***P < 0.001

**Figure 3. ALK3 activation is sufficient to promote the formation of adhesion sites and its recruitment to adhesion sites.** MEFsv40 cells co-expressing opto-ALK3-RFP/opto-β3 integrin-Venus, opto-ALK3Ca (constitutively active)-RFP/opto-β3 integrin-Venus, or opto-ALK3Ci (constitutively inactive)-RFP/opto-β3 integrin-Venus were seeded onto (A) poly-lysine (PLL), (B) vitronectin (VTN), or (C) fibronectin (FN)-coated substrates, then treated or not with sBMP2, and observed by TIRF-mode imaging. (D) Opto-ALK3Ca colocalized with β3 integrin

when cells were spread onto VTN and FN without sBMP2. The presence of sBMP2 led to an increase in the colocalization index of opto-ALK3 and opto-ALK3Ca with β3 integrin at adhesion sites. Of note, the presence of sBMP2 was unable to induce opto-ALK3 or opto-ALK3Ca relocalization if β3 integrin was not engaged (e.g., PLL-coated surfaces). (E) Opto-ALK3Ca, identified by β3 integrin-Venus, was able to induce the formation of FAs on PLL-coated substrates independently of sBMP2. N= 20 cells per condition. Scale bar 15 μm. Unpaired T test *0.05 >P > 0.01, **0.01 > P> 0.001, ***0.001 > P< 0.0001, ****0.00001 > P

**Figure 4. Optogenetic control of BMPRs with β3 integrin maintains the recruitment of ALK3 to focal adhesion sites and the exclusion of BMPRII from focal adhesions. (**A-B) Representative images of MEFsv40 cells co-expressing opto-CAAX/opto-β3 integrin, opto-ALK3/ opto-β3 integrin, opto-BMPRII/opto-β3 integrin, opto-ALK3Ca/opto-β3 integrin, or opto-ALK3Ci/opto-β3 integrin observed by TIRF imaging (A) before and (B) after pulses of blue laser light stimulation for 3 min (10-s frequency) to induce proximity between BMPRs and β3 integrin by the iLID/SspB system. Opto-CAAX and all opto-ALK3s were recruited to β3 integrin-containing FAs, whereas opto-BMPRII was not recruited. (C) The normalized intensity profile in FA sites shows the increase in RFP fluorescence intensity over time following the pattern of blue light illumination. Opto-ALK3Ca shows the highest recruitment level in FAs, whereas that of opto-CAAX and opto-ALK3Ci is three times lower. The mean ± SD is shown for 10 cells. Scale bar 15 μm.

**Figure 5. The targeting of ALK3 to focal adhesions upon BMP2 treatment leads to decreased ALK3 lateral mobility**. Opto-CAAX-RFP/opto-β3 integrin-Venus, opto-ALK3-RFP/opto-β3 integrin-Venus, or opto-BMPRII-RFP/opto-β3 integrin-Venus were co-expressed in REF52 cells. (A) Representative image of fluorescent recovery After photobleaching (FRAP) experimental setup of opto-ALK3-RFP immobilized within FAs upon sBMP2 treatment in the dark or without BMP2 but under blue light stimulation. A region of interest (ROI) close to FA (white circle) is bleached and monitored for fluorescence recovery. (B) The FRAP data are presented as the fitted curve of a single exponential equation, with background and bleaching correction, under basal conditions and sBMP2 and blue light stimulation. FRAP experiments were performed with total photobleaching at t = 0. The mean ± SD is shown for 10 cells. (C) The characteristic time of recovery (1/τ) was plotted for all conditions. Only the ALK3 recovery time was reduced after sBMP2 or blue light stimulation. (D) FRAP analysis by

limiting the ROI within and outside FAs shows a decrease in ALK3 lateral mobility within FA sites. Scale bar 15 µm. Unpaired T test, *0.05 > P > 0.01, **0.01> P > 0.001 ***0.001 > P < 0.0001

**Figure 6. sBMP2 treatment induces ALK3 immobilization within and outside FAs**. (A) Super-resolution intensity image of mEos2-ALK3 within FAs of a MEF obtained by sptPALM (50 Hz, 16,000 frames) (left) (inset: fluorescence image of β3-integrin-GFP). Corresponding trajectories are color-coded to show their diffusion modes: diffusive (green), confined (yellow), and immobile (red) (right). (B) ALK3 diffusion analysis during sBMP2 treatment. (C) The evolution of trajectories within and outside of FAs were sorted and analyzed (see methods). Distribution of Log(D) within FA versus outside (mean for cells). The grey areas that include D values < 0.011 µm2.s-1 correspond to immobile trajectories. (D) Fraction of diffusive, confined, and immobile populations within versus outside FAs (mean ± s.e.m. for cells). (E) D values for free-diffusive events (mean ± s.e.m. for trajectories). (F) Enrichment in FAs (mean ± s.e.m. for cells) for ALK3, with or without sBMP2 (same color code). All results for each condition correspond to pooled data from several independent experiments: ALK3 (10 cells, 47,362 trajectories, 2,509,527 detections) and ALK3 + sBMP2 (10 cells, 83,460 trajectories, 4,147,397 detections).

**Figure 7. ALK3 is involved in cell adhesion and migration.** (A) Representative images and quantification of the C2C12 cell area after deletion of ALK3 or BMPRII. Deletion of ALK3 but not BMPRII reduced the spreading of C2C12 cells in soft PLL/HA films presenting matrix-bound-BMP2 (bBMP2). At least 100 cells were analyzed per well and plate. Three independent experiments (biological replicates) were performed with 2 technical replicates per experiment, making up a total of at least 400 cells per condition. Scale bar 50 µm. (B) Individual migration assay on PLL/HA films with bBMP2, showing that the deletion of ALK3 in C2C12 cells negatively affects the velocity and Euclidean distance travelled. Representative results from three independent experiments are presented as means ± SEM. N ≥ 15 cells per condition. (C) Proximity between opto-CAAX/opto-β3 integrin, opto-ALK3/opto-β3 integrin and opto–BMPRII/ opto-β3 integrin induced by blue laser stimulation in MEFsv40 cells seeded on soft films presenting or not bBMP2. Only ALK3/β3 integrin proximity stimulated by blue light was able to induce cell spreading independently of bBMP2. Scale bar 100 µm. (D) Quantification of the cell area for the experiment in panel C. Of note, opto-ALK3/opto-β3

integrin proximity optimized cell spreading when bBMP2 was presented. N ≥ 100 cells per condition. Unpaired t test, *0.05 > P > 0.01, ****0.00001 > P

**Figure 8. ALK3/β3 integrin proximity induced by blue light stimulation shows the optimization of SMAD 1/5 signaling**. MEFsv40 cells co-expressing Opto-CAAX-RFP/opto-β3 integrin-Venus, opto-ALK3-RFP/opto-β3 integrin-Venus, or opto-BMPRII-RFP/opto-β3 integrin-Venus were seeded onto glass before pSMAD 1/5 immunostaining. (A and C) Without sBMP2, opto-BMPR overexpression or blue light activation were not sufficient to induce the phosphorylation and translocation of SMAD 1/5 to the nucleus. (B and D) In the presence of sBMP2, the proximity between ALK3 and β3 integrin induced by blue light was able to increase SMAD 1/5 phosphorylation in the nucleus. Measurement of mean nuclear intensity: N ≥ 100 cells per condition. Unpaired t test, ****0.00001 > P. Scale bar 100 μm.

**Figure 9. Schematic representation of ALK3 partitioning within and outside focal adhesions.** BMP2 induces ALK3 re-distribution at the cell surface into different domains corresponding to two confined populations of ALK3: one is confined to discrete regions, namely FAs, in which BMPRII subunits show no tendency to cluster (left side), and the other is homogeneously immobilized in the plasma membrane outside of FAs, likely through its association with BMPRII (right side). Integrin αVβ3 is a FN receptor, that recognizes the tripeptide cell-binding site Arg-Gly-Asp (RGD) located in the FN 7-10 domain. FN acts as a scaffold upon which the bioavailability and activity of several growth factors, including BMP2, is orchestrated through their interaction with the FN 12-14 domain. The close proximity between the integrin-binding and BMP2-binding domains of fibronectin favors proximity between ALK3 and β3 integrin in FAs. Exclusive ALK3 enrichment within FAs requires both BMP2 and integrin engagement to the extracellular matrix. Smad signaling requires ALK3, BMPRII, and β3 integrins (right side), whereas cell adhesive processes (spreading and migration) rely solely on ALK3 and β3 integrins (left side). The asterisk, circle or square positioned at the intracellular domain of ALK3 indicate a conformational change which might be crucial to expose sites of phosphorylation or provide a docking site for specific kinases or signaling molecules to control ALK3 recruitment outside and within FAs.

**Figure S1. Selection of mesenchymal (C2C12, MEFsv40, REF52) and epithelial (EPH4) cell lines to study BMP2 receptor dynamics.** The ability of the cell lines to respond to soluble

BMP2 stimulation was validated by the phosphorylation and nuclear translocation of SMAD 1/5 after 4 h of treatment by (A) immunoblotting and (B) immunofluorescence visualized by confocal microscopy. Quantification of nuclear P-Smad: N ≥ 100 cells per condition. Scale bar: 100 µm. (C) Immunoblots of opto-BMPRs and opto-β3 Integrin showing expression of the opto-proteins at the expected molecular weight. (D) Improvement of the visualization of transmembrane BMPR by total internal reflection microscopy (TIRFM) by examining a thin section of the sample at the adherent cell surface relative to confocal microscopy. Opto-β3 integrin is observed within the FA sites. Scale bar 15 µm. Source data are available for this figure: SourceData FS1.

**Figure S2. The spatial organization of ALK3 in adhesion sites is observed in different cell types and does not require BMPRII.** In (A) REF52 and (B) C2C12 cells without BMP2 treatment, BMPRs were distributed throughout the cell surface and opto-β3 integrin-Venus was targeted within FAs observed on TIRFM. sBMP2 treatment induced the recruitment of ALK3 to FAs, whereas BMPRII remained mainly excluded. Scale bar 15 µm. C. The deletion of BMPRII does not impair ALK3 recruitment in focal adhesions. MEF cells are depleted either in BMPRII, ActRIIA, ActRIIB or all receptors before measuring the level of ALK3 recruitment in FA after BMP2 stimulation. Scr: scramble. N ≥ 136 cells per condition.

**Figure S3. Binding properties of BMP2.** In vitro binding between BMP2, ALK3 and BMP-type II, receptors quantified using biolayer interferometry. (A) Example of kinetic experiment of BMP2 binding to immobilized ALK3 receptor. BMP2 was added at increasing concentrations, let interact and then removed from the solution. (B) Kinetic experiment of BMP2 binding to immobilized BMPR-II receptor. (C) The association constant (ka) was deduced from the fit of the kinetic data for the four studied receptors. (D) The dissociation constant (kd) was deduced from the fit of the kinetic data. (E) Summary table of the equilibrium constant Kd of BMP2 interaction with all four BMP receptors. Note the better affinity of ALK3 for BMP2. The results are representative of three independent experiments. (F) BMP2 interacts with vitronectin. Interaction between recombinant BMP2 and the proteins vitronectin and bovine serum albumin was measured by ELISA. Increasing concentrations of vitronectin or BSA were incubated for 1 h in PBS at 37 °C in contact with BMP2 coated 96-well plate. The absorbance at 450 nm is plotted in function of the initial BMP2 concentration used to coat the multi-well

plate. The figure illustrates one representative experiment of two performed, giving similar results.

**Figure S4. Induction of the proximity between ALK3 and β3 integrin in mesenchymal and epithelial cell lines.** (A) Representative images showing ALK3 targeting FAs after 3 min of blue light stimulation in the C2C12, MEsv40, REF52, and Eph4 cell lines. Scale bar 15 μm. (B) Profile of the normalized increase in intensity of opto-ALK3-RFP at FA sites over time upon blue-light illumination. All mesenchymal and epithelial cell lines showed a similar recruitment profile. The mean ± SD is shown for 10 cells.

**Figure S5: Identification of signaling pathways required for maintaining cell spreading and Smad signaling induced by BMP2** (A) C2C12 cells were transfected with siRNA against the BMP receptors ALK3 and BMPRII and against the kinases Src, FAK and ILK, then plated on rigid films with matrix-bound BMP2 for 4 h. The spreading area were quantified after cell staining with actin. The relative cell spreading is expressed in %, in comparison to a control scrambled siRNA. Data represent the mean ± SEM, with three biological replicates and two technical replicates per experiment. Cell number ≥ 500 per condition. (B-C) Relationship between ALK3 and integrin signaling. Cells are plated onto glass coverslips coated with Fibronectin (FN) or Vitronectin (VTN) before staining with phalloidin and β3 integrin. ALK3 controls both (B) cell spreading and (C) the area of FAs, as shown by the effect of SiRNA treatment against ALK3 relative to SiScr or SiBMPRII treatment. Cell number ≥ 98 per condition. FA number ≥ 824 per condition (D) Enrichment of FA in ALK3 upon BMP2 stimulation. Whereas ALK3 recruitment is not affected by the deletion of Src and FAK kinases, ALK3 is more recruited in FA when ILK is deleted as compared to the control (Scr for Scramble). N ≥ 52 cells per condition. (E) Smad signaling is not correlated with cell area. A. Representation of pSMAD1/5/9 intensity as a function of cell spreading (express in μm2), for all cells included in the quantitative analysis, each point corresponding to a single cell. Upper graph: in the absence of BMP-2 and lower graph: on stiff films in the presence of matrix-bound BMP2. No clear correlation appears between both parameters. N ≥ 500 cells per condition. (F) Quantification of P-Smad and P-GSK3 after western blotting of cells deleted in ALK3 or BMPRII and treated with BMP2. GADPH is used as loading control. Deletion of ALK3 and not BMPRII deletion induces a loss of GSK3β phosphorylation.

**Video 1. Optogenetic control of CAAX/β3 integrin proximity leads to the recruitment of CAAX to focal adhesion sites.** MEFsv40 cells co-expressing opto-CAAX-RFP/β3 integrin-Venus imaged by total internal reflection microscopy. After stimulation with a blue laser (488 nm) for 3 min (10-s frequency), CAAX is targeted to β3 integrin-containing FAs. Composite images of CAAX and β3 integrin show colocalization at adhesion sites. (6 min, 7 frames per second). Scale bar 15 μm.

**Video 2. Optogenetic control of ALK3/β3 integrin proximity leads to the recruitment of ALK3 to focal adhesion sites.** MEFsv40 cells co-expressing opto-ALK3-RFP/opto-β3 integrin-Venus were imaged by total internal reflection microscopy. After stimulation with a blue laser (488 nm) for 3 min (10-s frequency), ALK3 is targeted to β3 integrin-FAs. Composite images of ALK3 and β3 integrin show colocalization at adhesion sites (7 frames per second). Scale bar 15 μm.

**Video 3. Optogenetic control of BMPRII/ β3 integrin proximity reveals the exclusion of BMPRII from focal adhesion sites.** MEFsv40 cells co-expressing opto-BMPRII-RFP/opto-β3 integrin-Venus were imaged by total internal reflection microscopy. After stimulation with a blue laser (488 nm) for 3 min (10-s frequency), BMPRII is not recruited to β3 integrin-containing FAs. Composite images of BMPRII and β3 integrin show the exclusion of BMPRII exclusion from adhesion sites (7 frames per second). Scale bar 15 μm.

**Video 4. Optogenetic control of ALK3Ca/β3 integrin proximity leads to the recruitment of ALK3Ca to focal adhesion sites.** MEFsv40 cells co-expressing opto-ALK3Ca-RFP/opto-β3 integrin-Venus were imaged by total internal reflection microscopy. After stimulation with a blue laser (488 nm) for 3 min (10-s frequency), ALK3Ca is recruited to β3 integrin-containing FAs. Composite images of ALK3Ca and β3 integrin show colocalization at adhesion sites. (7 frames per second). Scale bar 15 μm.

**Video 5. Optogenetic control of ALK3Ci/β3 integrin proximity shows limited recruitment of ALK3Ci to focal adhesion sites.** MEFsv40 cells co-expressing opto-ALK3Ci-RFP/β3 integrin-Venus were imaged by total internal reflection microscopy. After stimulation with a blue laser (488 nm) for 3 min (10-s frequency), ALK3Ci shows a lower capacity to be recruited to β3 integrin-containing FAs. Composite images of ALK3Ci and β3 integrin show colocalization at adhesion sites. (7 frames per second). Scale bar 15 μm.

**Video 6. C2C12 cells co-expressing opto-ALK3-RFP/β3 integrin-Venus.** After stimulation with a blue laser (488 nm) for 3 min (10-s frequency), ALK3 is recruited to β3 integrin-containing FAs. Composite images of ALK3 and β3 integrin show colocalization at adhesion sites (7 frames per second). Scale bar 15 μm.

**Video 7. MEFsv40 cells co-expressing opto-ALK3-RFP/β3 integrin-Venus.** After stimulation with a blue laser (488 nm) for 3 min (10-s frequency), ALK3 is recruited to β3 integrin-containing FAs. Composite images of ALK3 and β3 integrin show colocalization at adhesion sites (7 frames per second). Scale bar 15 μm.

**Video 8. REF52 cells co-expressing opto-ALK3-RFP/β3 integrin-Venus.** After stimulation with a blue laser (488 nm) for 3 min (10-s frequency), ALK3 is recruited to β3 integrin-containing FAs. Composite images of ALK3 and β3 integrin show colocalization at adhesion sites (7 frames per second). Scale bar 15 μm

**Video 9. Eph4 cells co-expressing opto-ALK3-RFP/β3 integrin-Venus.** After stimulation with a blue laser (488 nm) for 3 min (10-s frequency), ALK3 is recruited to β3 integrin-containing FAs. Composite images of ALK3 and β3 integrin show colocalization at adhesion sites. (7 frames per second). Scale bar 15μm.

**Supplementary Table S.1. Primer sequences used for sequencing (F): forward, (R): reverse. ECD: extracellular domain.**

**Supplementary Table S2. Primer Sequences used in qPCR**

**References**


Aragón, E., N. Goerner, A.I. Zaromytidou, Q. Xi, A. Escobedo, J. Massagué, and M.J. Macias. 2011. A smad action turnover switch operated by WW domain readers of a phosphoserine code. *Genes Dev.* 25:1275–1288. doi:10.1101/gad.2060811.

Banjade, S., and M.K. Rosen. 2014. Phase transitions of multivalent proteins can promote clustering of membrane receptors. *Elife*. 3. doi:10.7554/eLife.04123.

Bolte, S., and F.P. Cordelières. 2006. A guided tour into subcellular colocalization analysis in light microscopy. *J. Microsc.* 224:213–232. doi:10.1111/j.1365-2818.2006.01706.x.

Chazeau, A., A. Mehidi, D. Nair, J.J. Gautier, C. Leduc, I. Chamma, F. Kage, A. Kechkar, O. Thoumine, K. Rottner, D. Choquet, A. Gautreau, J.-B. Sibarita, and G. Giannone. 2014. Nanoscale segregation of actin nucleation and elongation factors determines dendritic spine protrusion. *EMBO J.* 33:2745–64. doi:10.15252/embj.201488837.

Chong, P.A., and J.D. Forman-Kay. 2016. Liquid–liquid phase separation in cellular signaling systems. *Curr. Opin. Struct. Biol.* 41:180–186. doi:10.1016/j.sbi.2016.08.001.

Comoglio, P.M., C. Boccaccio, and L. Trusolino. 2003. Interactions between growth factor receptors and adhesion molecules: breaking the rules. *Curr. Opin. Cell Biol.* 15:565–71.

Crouzier, T., L. Fourel, T. Boudou, C. Albiges-Rizo, and C. Picart. 2011. Presentation of BMP-2 from a soft biopolymeric film unveils its activity on cell adhesion and migration. *Adv Mater*. 23:H111-8. doi:10.1002/adma.201004637.

Delcommenne, M., C. Tan, V. Gray, L. Rue, J. Woodgett, and S. Dedhar. 1998. Phosphoinositide-3-OH kinase-dependent regulation of glycogen synthase kinase 3 and protein kinase B/AKT by the integrin-linked kinase. *Proc. Natl. Acad. Sci. U. S. A.* 95:11211–11216. doi:10.1073/pnas.95.19.11211.

Fourel, L., A. Valat, E. Faurobert, R. Guillot, I. Bourrin-Reynard, K. Ren, L. Lafanechère, E. Planus, C. Picart, and C. Albiges-Rizo. 2016. β3 integrin-mediated spreading induced by matrix-bound BMP-2 controls Smad signaling in a stiffness-independent manner. *J. Cell Biol.* 212. doi:10.1083/jcb.201508018.

Fuentealba, L.C., E. Eivers, A. Ikeda, C. Hurtado, H. Kuroda, E.M. Pera, and E.M. De Robertis. 2007. Integrating Patterning Signals: Wnt/GSK3 Regulates the Duration of the BMP/Smad1 Signal. *Cell*. 131:980–993. doi:10.1016/j.cell.2007.09.027.

Gilboa, L., A. Nohe, T. Geissendörfer, W. Sebald, Y.I. Henis, and P. Knaus. 2000. Bone morphogenetic protein receptor complexes on the surface of live cells: A new oligomerization mode for serine/threonine kinase receptors. *Mol. Biol. Cell*. 11:1023–1035. doi:10.1091/mbc.11.3.1023.

Grusch, M., K. Schelch, R. Riedler, E. Reichhart, C. Differ, W. Berger, Á. Inglés-Prieto, and H. Janovjak. 2014. Spatio-temporally precise activation of engineered receptor tyrosine kinases by light. *EMBO J.* 33:1713–1726. doi:10.15252/embj.201387695.

Guntas, G., R.A. Hallett, S.P. Zimmerman, T. Williams, H. Yumerefendi, J.E. Bear, and B.

Kuhlman. 2015. Engineering an improved light-induced dimer (iLID) for controlling the localization and activity of signaling proteins. *Proc. Natl. Acad. Sci. U. S. A.* 112:112–117. doi:10.1073/pnas.1417910112.

Guo, X., and X.F. Wang. 2009. Signaling cross-talk between TGF-β/BMP and other pathways. *Cell Res.* 19:71–88. doi:10.1038/cr.2008.302.

Guzman, A., M. Zelman-Femiak, J.H. Boergermann, S. Paschkowsky, P.A. Kreuzaler, P. Fratzl, G.S. Harms, and P. Knaus. 2012. SMAD versus non-SMAD signaling is determined by lateral mobility of Bone Morphogenetic Protein (BMP) receptors. *J. Biol. Chem.* 287:39492–39504. doi:10.1074/jbc.M112.387639.

Hartung, A., K. Bitton-Worms, M.M. Rechtman, V. Wenzel, J.H. Boergermann, S. Hassel, Y.I. Henis, and P. Knaus. 2006. Different Routes of Bone Morphogenic Protein (BMP) Receptor Endocytosis Influence BMP Signaling. *Mol. Cell. Biol.* 26:7791–7805. doi:10.1128/mcb.00022-06.

Hiepen, C., J. Jatzlau, S. Hildebrandt, B. Kampfrath, M. Goktas, A. Murgai, J.L. Cuellar Camacho, R. Haag, C. Ruppert, G. Sengle, E.A. Cavalcanti-Adam, K.G. Blank, and P. Knaus. 2019. BMPR2 acts as a gatekeeper to protect endothelial cells from increased TGFβ responses and altered cell mechanics. *PLoS Biol.* 17. doi:10.1371/journal.pbio.3000557.

Hoodless, P.A., T. Haerry, S. Abdollah, M. Stapleton, M.B. O'Connor, L. Attisano, and J.L. Wrana. 1996. MADR1, a MAD-related protein that functions in BMP2 signaling pathways. *Cell*. 85:489–500. doi:10.1016/S0092-8674(00)81250-7.

Hynes, R.O. 2009. The extracellular matrix: not just pretty fibrils. *Science*. 326:1216–9. doi:10.1126/science.1176009.

Ivaska, J., and J. Heino. 2011. Cooperation between integrins and growth factor receptors in signaling and endocytosis. *Annu. Rev. Cell Dev. Biol.* 27:291–320. doi:10.1146/annurev-cellbio-092910-154017.

Khodr, V., P. Machillot, E. Migliorini, J.-B. Reiser, and C. Picart. 2021. High-throughput measurements of bone morphogenetic protein/bone morphogenetic protein receptor interactions using biolayer interferometry. *Biointerphases*. 16:031001. doi:10.1116/6.0000926.

Kim, W.K., Y. Kwon, M. Jang, M. Park, J. Kim, S. Cho, D.G. Jang, W. Bin Lee, S.H. Jung, H.J. Choi, B.S. Min, T. Il Kim, S.P. Hong, Y.K. Paik, and H. Kim. 2019. β-catenin activation down-regulates cell-cell junction-related genes and induces epithelial-to-mesenchymal transition in colorectal cancers. *Sci. Rep.* 9. doi:10.1038/s41598-019-54890-9.

Klumpe, H.E., M.A. Langley, J.M. Linton, C.J. Su, Y.E. Antebi, M.B. Elowitz, H.E. Klumpe, M.A. Langley, J.M. Linton, C.J. Su, and Y.E. Antebi. 2022. Article The context-dependent , combinatorial logic of BMP signaling ll The context-dependent , combinatorial logic of BMP signaling. *Cell Syst.* 13:388-407.e10. doi:10.1016/j.cels.2022.03.002.

Leduc, C., S. Si, J. Gautier, M. Soto-Ribeiro, B. Wehrle-Haller, A. Gautreau, G. Giannone, L. Cognet, and B. Lounis. 2013. A highly specific gold nanoprobe for live-cell single-molecule imaging. *Nano Lett.* 13:1489–1494. doi:10.1021/nl304561g.

Li, P., S. Banjade, H.C. Cheng, S. Kim, B. Chen, L. Guo, M. Llaguno, J. V. Hollingsworth, D.S. King, S.F. Banani, P.S. Russo, Q.X. Jiang, B.T. Nixon, and M.K. Rosen. 2012. Phase transitions in the assembly of multivalent signalling proteins. *Nature*. 483:336–340. doi:10.1038/nature10879.

Li, W., W. Li, L. Zou, S. Ji, C. Li, K. Liu, G. Zhang, Q. Sun, F. Xiao, and D. Chen. 2017. Membrane targeting of inhibitory Smads through palmitoylation controls TGF-β/BMP signaling. *Proc. Natl. Acad. Sci. U. S. A.* 114:13206–13211. doi:10.1073/pnas.1710540114.

Lorent, J.H., B. Diaz-Rohrer, X. Lin, K. Spring, A.A. Gorfe, K.R. Levental, and I. Levental. 2017. Structural determinants and functional consequences of protein affinity for membrane rafts. *Nat. Commun.* 8. doi:10.1038/s41467-017-01328-3.

Lorent, J.H., and I. Levental. 2015. Structural determinants of protein partitioning into ordered membrane domains and lipid rafts. *Chem. Phys. Lipids*. 192:23–32. doi:10.1016/j.chemphyslip.2015.07.022.

Machillot, P., C. Quintal, F. Dalonneau, L. Hermant, P. Monnot, K. Matthews, V. Fitzpatrick, J. Liu, I. Pignot-Paintrand, and C. Picart. 2018. Automated Buildup of Biomimetic Films in Cell Culture Microplates for High-Throughput Screening of Cellular Behaviors. *Adv. Mater.* 30. doi:10.1002/adma.201801097.

Manley, S., J.M. Gillette, G.H. Patterson, H. Shroff, H.F. Hess, E. Betzig, and J. Lippincott-Schwartz. 2008. High-density mapping of single-molecule trajectories with photoactivated localization microscopy. *Nat Methods*. 5:155.

Margadant, C., and A. Sonnenberg. 2010. Integrin–TGF-β crosstalk in fibrosis, cancer and wound healing. *EMBO Rep.* 11:97–105. doi:10.1038/embor.2009.276.

Márquez, M.G., and N.B. Sterin-Speziale. 2008. Is DRM lipid composition relevant in cell-extracellular matrix adhesion structures? *Cell Adh. Migr.* 2:180–183. doi:10.4161/cam.2.3.6604.

Martin, I.M., M.M. Nava, S.A. Wickström, and F. Gräter. 2022. ATP allosterically stabilizes integrin-linked kinase for efficient force generation. *Proc. Natl. Acad. Sci. U. S. A.* 119. doi:10.1073/pnas.2106098119.

Martino, M.M., P.S. Briquez, E. Güç, F. Tortelli, W.W. Kilarski, S. Metzger, J.J. Rice, G.A. Kuhn, R. Müller, M.A. Swartz, and J.A. Hubbell. 2014. Growth factors engineered for super-affinity to the extracellular matrix enhance tissue healing. *Science*. 343:885–8. doi:10.1126/science.1247663.

Mehidi, A., O. Rossier, A. Chazeau, F. Biname, A. Remorino, M. Coppey, Z. Karatas, J.-B. Sibarita, V. Moreau, G. Giannone, F. Binamé, and A. Remorino. 2017. Fast Activation Cycles Of Rac1 At The Lamellipodium Tip Trigger Membrane Protrusion. *bioRxiv*. doi:10.1101/130849.

Migliorini, E., A. Guevara-Garcia, C. Albiges-Rizo, and C. Picart. 2020. Learning from BMPs and their biophysical extracellular matrix microenvironment for biomaterial design. *Bone*. 141. doi:10.1016/j.bone.2020.115540.

Nickel, J., and T.D. Mueller. 2019. Specification of BMP Signaling. *Cells*. 8. doi:10.3390/cells8121579.

Nohe, A., S. Hassel, M. Ehrlich, F. Neubauer, W. Sebald, Y.I. Henis, and P. Knaus. 2002. The mode of bone morphogenetic protein (BMP) receptor oligomerization determines different BMP-2 signaling pathways. *J. Biol. Chem.* 277:5330–5338. doi:10.1074/jbc.M102750200.

Orré, T., A. Joly, Z. Karatas, B. Kastberger, C. Cabriel, R.T. Böttcher, S. Lévêque-Fort, J.B. Sibarita, R. Fässler, B. Wehrle-Haller, O. Rossier, and G. Giannone. 2021. Molecular motion and tridimensional nanoscale localization of kindlin control integrin activation in focal adhesions. *Nat. Commun.* 12. doi:10.1038/s41467-021-23372-w.

Owens, P., M.W. Pickup, S. V. Novitskiy, J.M. Giltnane, A.E. Gorska, C.R. Hopkins, C.C. Hong, and H.L. Moses. 2015. Inhibition of BMP signaling suppresses metastasis in mammary cancer. *Oncogene*. 34:2437–2449. doi:10.1038/onc.2014.189.

Owens, P., M.W. Pickup, S. V Novitskiy, A. Chytil, A.E. Gorska, M.E. Aakre, J. West, and H.L. Moses. 2012. Disruption of bone morphogenetic protein receptor 2 (BMPR2) in mammary tumors promotes metastases through cell autonomous and paracrine mediators. *Proc. Natl. Acad. Sci. U. S. A.* 109:2814–9. doi:10.1073/pnas.1101139108.

Owens, T.W., R.L. Rogers, S. Best, A. Ledger, A.-M. Mooney, A. Ferguson, P. Shore, A. Swarbrick, C.J. Ormandy, P.T. Simpson, J.S. Carroll, J. Visvader, and M.J. Naylor. 2014. Runx2 is a novel regulator of mammary epithelial cell fate in development and breast cancer. *Cancer Res.* 74:5277–5286. doi:10.1158/0008-5472.CAN-14-0053.

Pande, G. 2000. The role of membrane lipids in regulation of integrin functions. *Curr. Opin. Cell Biol.* 12:569–574. doi:10.1016/S0955-0674(00)00133-2.

Perk, J., A. Iavarone, and R. Benezra. 2005. Id family of helix-loop-helix proteins in cancer. *Nat. Rev. Cancer*. 5:603–614. doi:10.1038/nrc1673.

Przybyla, L., J.N. Lakins, and V.M. Weaver. 2016. Tissue Mechanics Orchestrate Wnt-Dependent Human Embryonic Stem Cell Differentiation. *Cell Stem Cell*. 19:462–475. doi:10.1016/j.stem.2016.06.018.

Rajski, M., A. Saaf, and M. Buess. 2015. BMP2 response pattern in human lung fibroblasts predicts outcome in lung adenocarcinomas. *BMC Med. Genomics*. 8:16. doi:10.1186/s12920-015-0090-4.

Rossier, O., V. Octeau, J.-B. Sibarita, C. Leduc, B. Tessier, D. Nair, V. Gatterdam, O. Destaing, C. Albigès-Rizo, R. Tampé, L. Cognet, D. Choquet, B. Lounis, and G. Giannone. 2012. Integrins β1 and β3 exhibit distinct dynamic nanoscale organizations inside focal adhesions. *Nat. Cell Biol.* 14:1057–67. doi:10.1038/ncb2588.

Rothhammer, T., I. Poser, F. Soncin, F. Bataille, M. Moser, and A.K. Bosserhoff. 2005. Bone morphogenic proteins are overexpressed in malignant melanoma and promote cell invasion and migration. *Cancer Res.* 65:448–456.

Rys, J.P., C.C. DuFort, D.A. Monteiro, M.A. Baird, J.A. Oses-Prieto, S. Chand, A.L. Burlingame, M.W. Davidson, and T.N. Alliston. 2015. Discrete spatial organization of TGFβ receptors couples receptor multimerization and signaling to cellular tension. *Elife*. 4. doi:10.7554/eLife.09300.

Sakai, T., S. Li, D. Docheva, C. Grashoff, K. Sakai, G. Kostka, A. Braun, A. Pfeifer, P.D.

Yurchenco, and R. Fässler. 2003. Integrin-linked kinase (ILK) is required for polarizing the epiblast, cell adhesion, and controlling actin accumulation. *Genes Dev.* 17:926–940. doi:10.1101/gad.255603.

Sales, A., V. Khodr, P. Machillot, L. Chaar, L. Fourel, A. Guevara-Garcia, E. Migliorini, C. Albigès-Rizo, and C. Picart. 2022. Differential bioactivity of four BMP-family members as function of biomaterial stiffness. *Biomaterials*. 281. doi:10.1016/j.biomaterials.2022.121363.

Sánchez-Duffhues, G., C. Hiepen, P. Knaus, and P. ten Dijke. 2015. Bone morphogenetic protein signaling in bone homeostasis. *Bone*. 80:43–59. doi:10.1016/j.bone.2015.05.025.

Schindelin, J., I. Arganda-Carreras, E. Frise, V. Kaynig, M. Longair, T. Pietzsch, S. Preibisch, C. Rueden, S. Saalfeld, B. Schmid, J.-Y.J.-Y. Tinevez, D.J. White, V. Hartenstein, K. Eliceiri, P. Tomancak, A. Cardona, K. Liceiri, P. Tomancak, and C. A. 2012. Fiji: An open source platform for biological image analysis. *Nat. Methods*. 9:676–682. doi:10.1038/nmeth.2019.Fiji.

Shepherd, T.G., M.L. Mujoomdar, and M.W. Nachtigal. 2010. Constitutive activation of BMP signalling abrogates experimental metastasis of OVCA429 cells via reduced cell adhesion. *J. Ovarian Res.* 3:5. doi:10.1186/1757-2215-3-5.

Stanchi, F., C. Grashoff, C.F.N. Yonga, D. Grall, R. Fässler, and E. Van Obberghen-Schilling. 2009. Molecular dissection of the ILK-PINCH-parvin triad reveals a fundamental role for the ILK kinase domain in the late stages of focal-adhesion maturation. *J. Cell Sci.* 122:1800–1811. doi:10.1242/jcs.044602.

Vaynberg, J., K. Fukuda, F. Lu, K. Bialkowska, Y. Chen, E.F. Plow, and J. Qin. 2018. Non-catalytic signaling by pseudokinase ILK for regulating cell adhesion. *Nat. Commun.* 9. doi:10.1038/s41467-018-06906-7.

Wegleiter, T., K. Buthey, D. Gonzalez-Bohorquez, M. Hruzova, M.K. bin Imtiaz, A. Abegg, I. Mebert, A. Molteni, D. Kollegger, P. Pelczar, and S. Jessberger. 2019. Palmitoylation of BMPR1a regulates neural stem cell fate. *Proc. Natl. Acad. Sci. U. S. A.* 116:25688–25696. doi:10.1073/pnas.1912671116.

Wieser, R., J.L. Wrana, and J. Massagué. 1995. GS domain mutations that constitutively activate TβR-I, the downstream signaling component in the TGF-β receptor complex. *EMBO J.* 14:2199–2208. doi:10.1002/j.1460-2075.1995.tb07214.x.

Yadin, D., P. Knaus, and T.D. Mueller. 2016. Cytokine & Growth Factor Reviews Structural insights into BMP receptors : Speci fi city , activation and inhibition. *Cytokine Growth Factor Rev.* 27:13–34. doi:10.1016/j.cytogfr.2015.11.005.

Zhang, Y.E. 2009. Non-Smad pathways in TGF-β signaling. *Cell Res.* 19:128–139. doi:10.1038/cr.2008.328.

Zhou, D.W., M.A. Fernández-Yagüe, E.N. Holland, A.F. García, N.S. Castro, E.B. O'Neill, J. Eyckmans, C.S. Chen, J. Fu, D.D. Schlaepfer, and A.J. García. 2021. Force-FAK signaling coupling at individual focal adhesions coordinates mechanosensing and microtissue repair. *Nat. Commun.* 12. doi:10.1038/s41467-021-22602-5.

Figure 1. Guevara-Garcia *et al.*

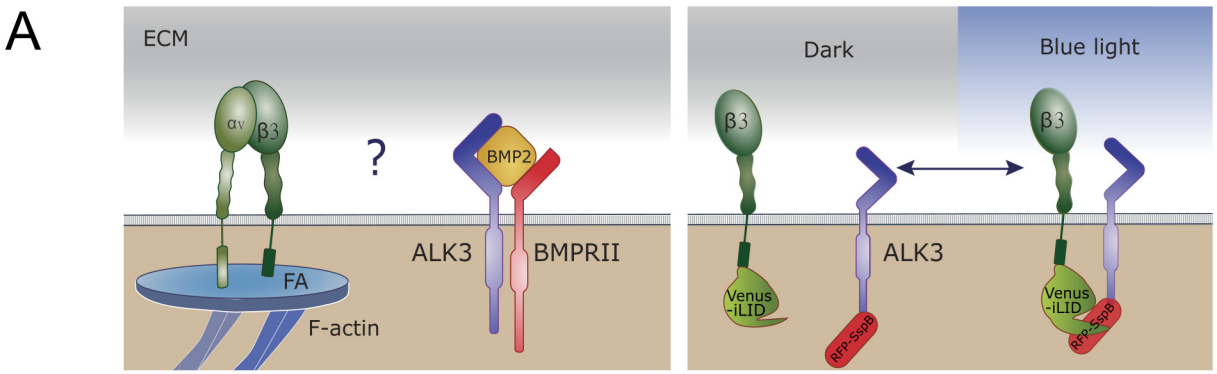


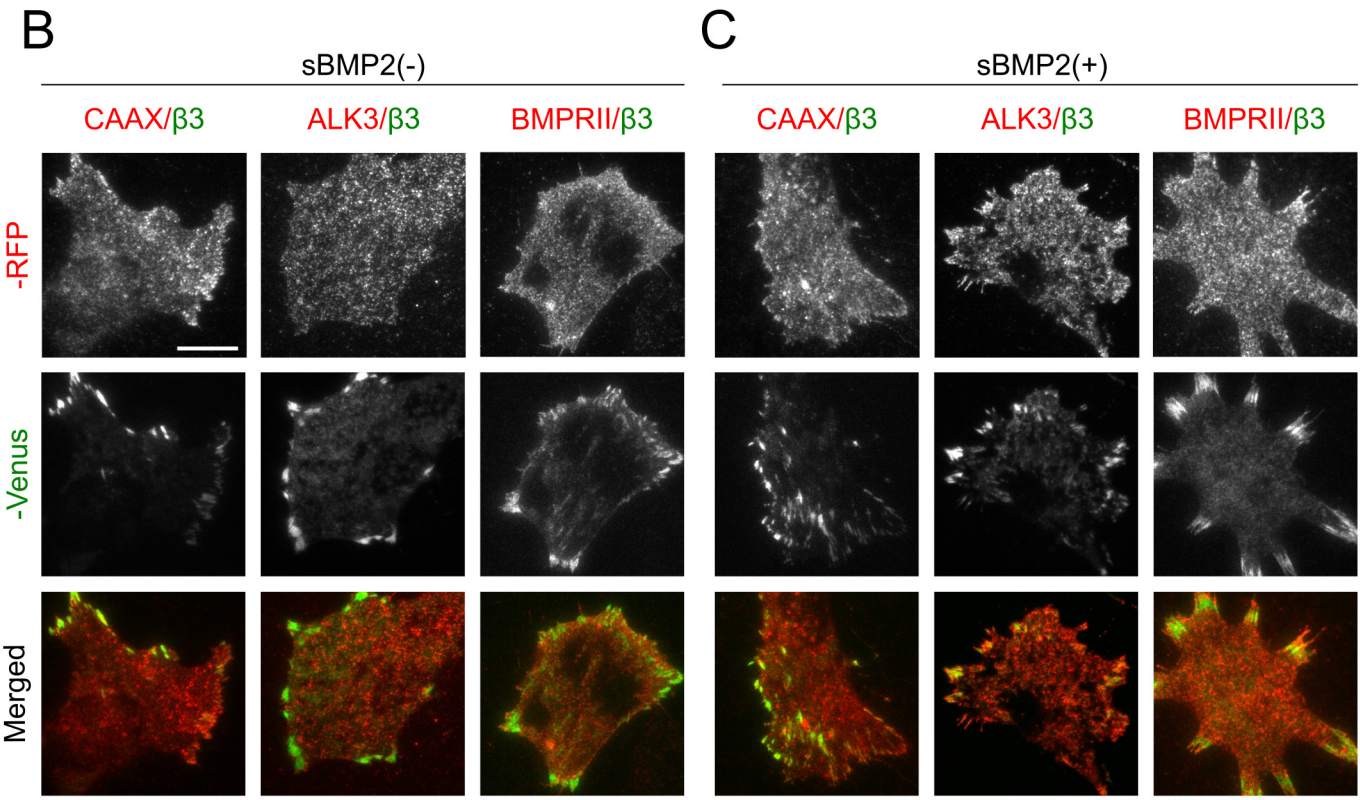


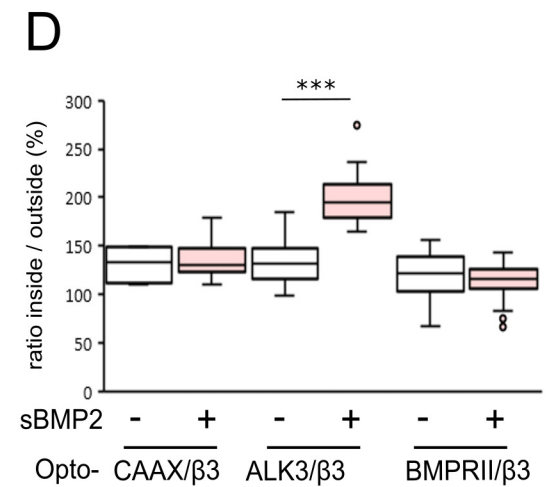

# Figure 2. Guevara-Garcia *et al.*

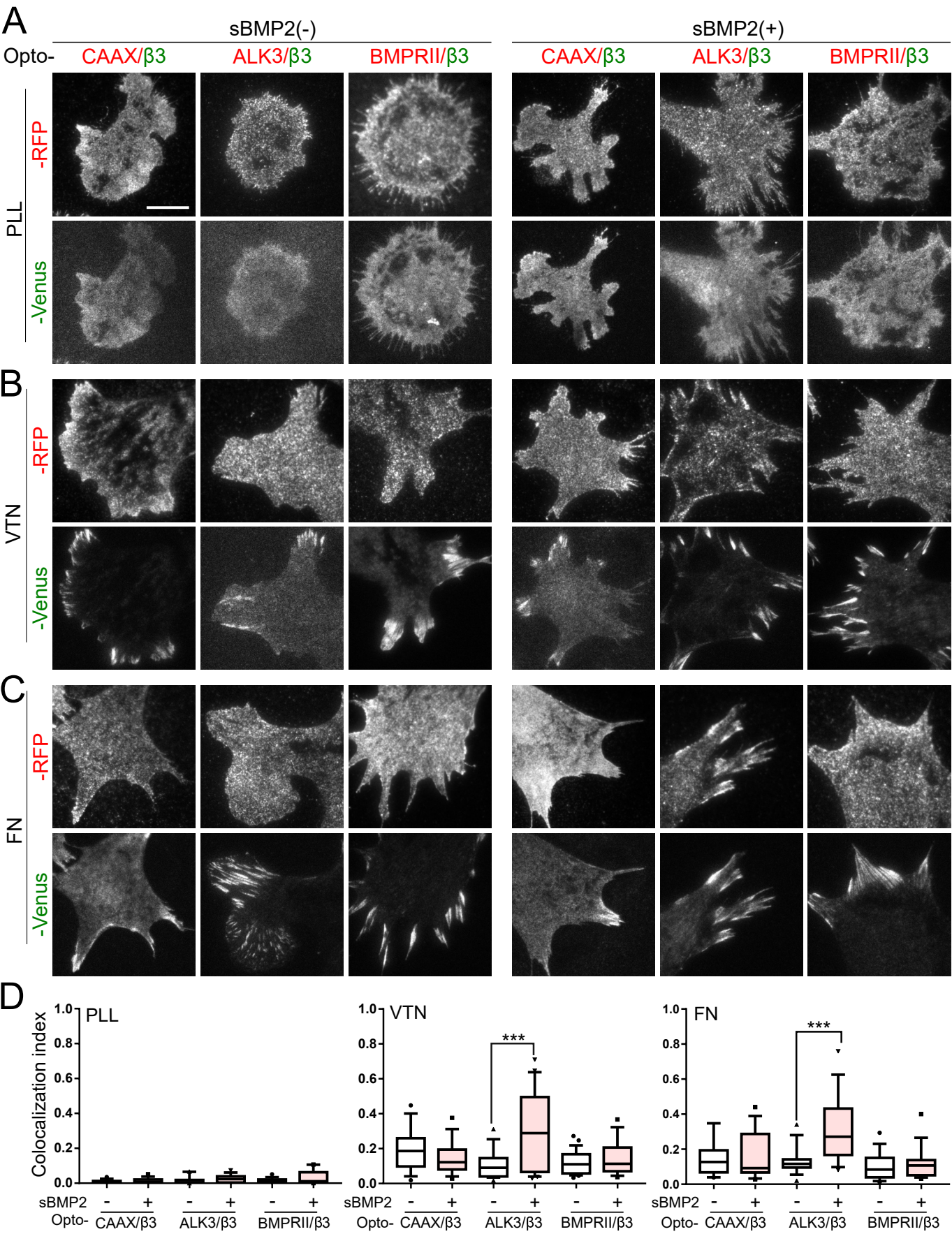

# Figure 3. Guevara-Garcia *et al.*

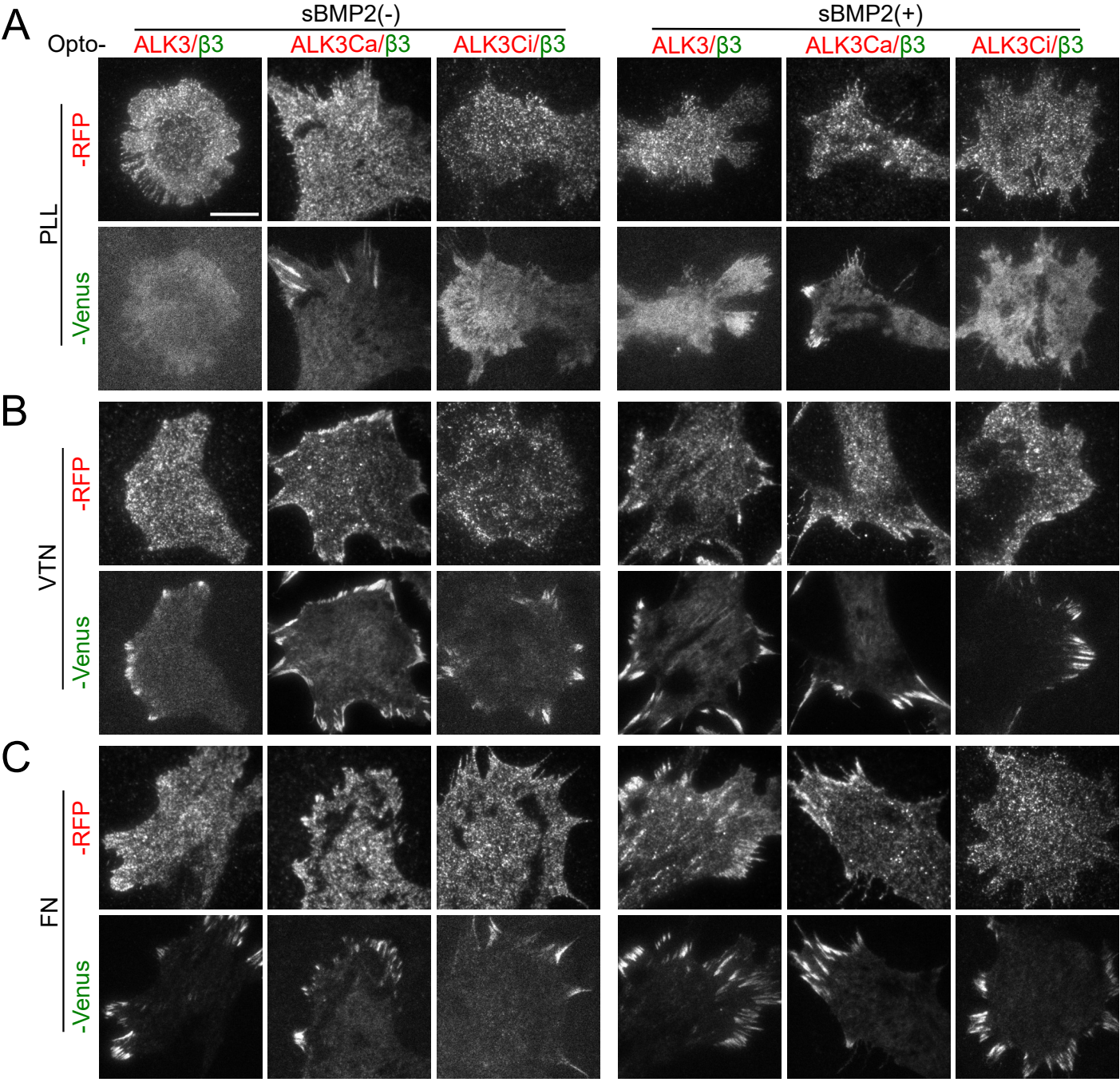


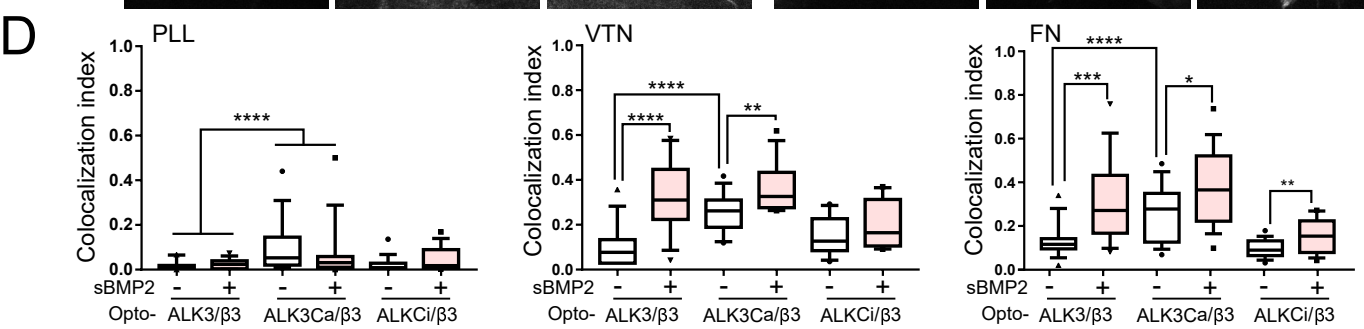


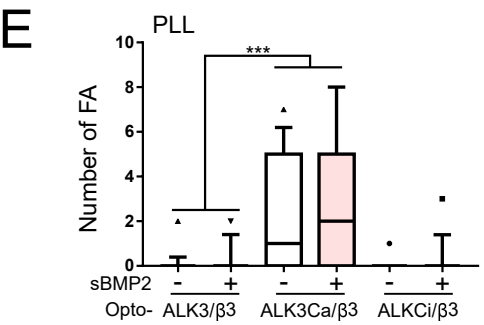

Figure 4. Guevara-Garcia *et al.*

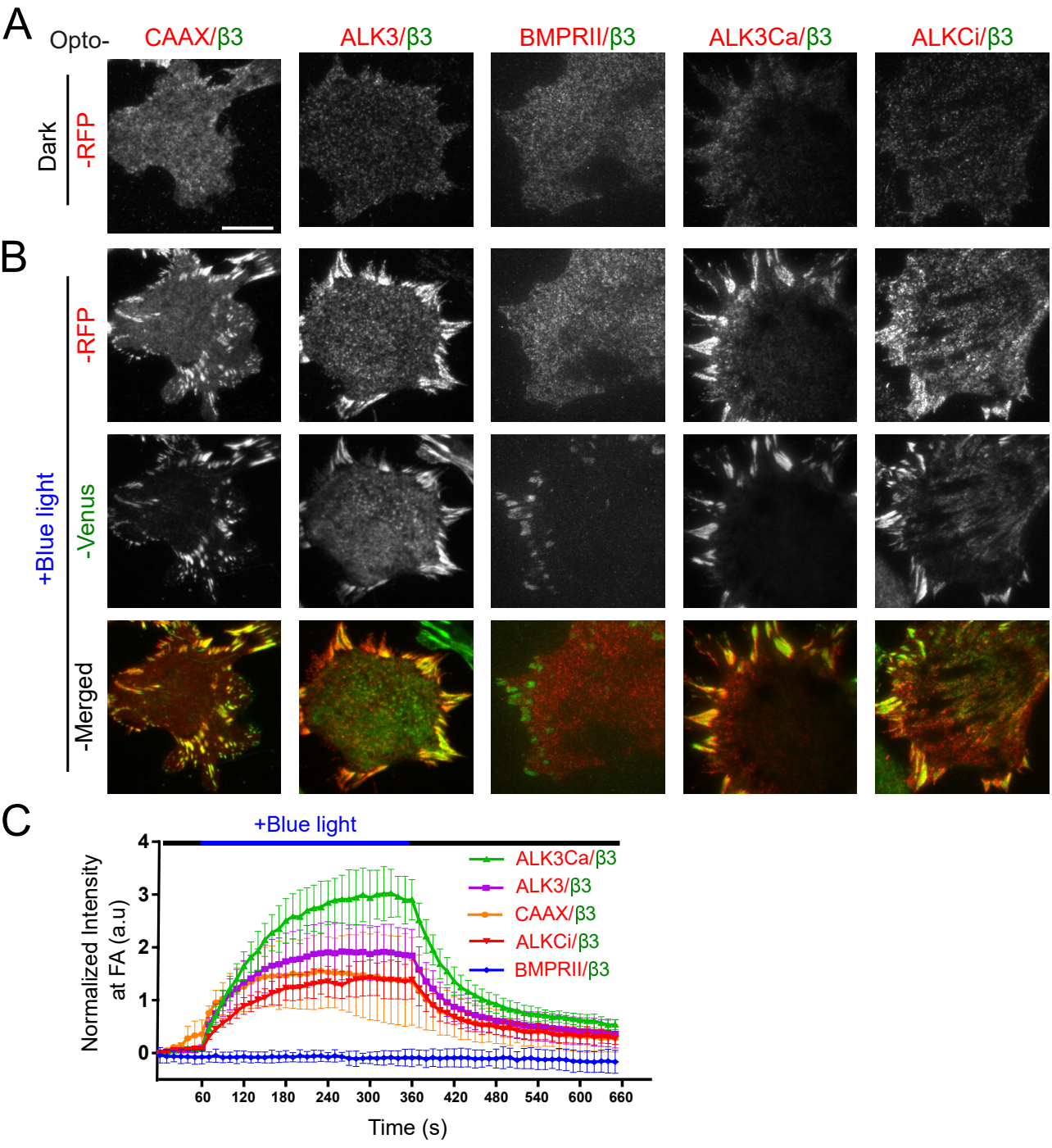

# Figure 5. Guevara-Garcia *et al.*

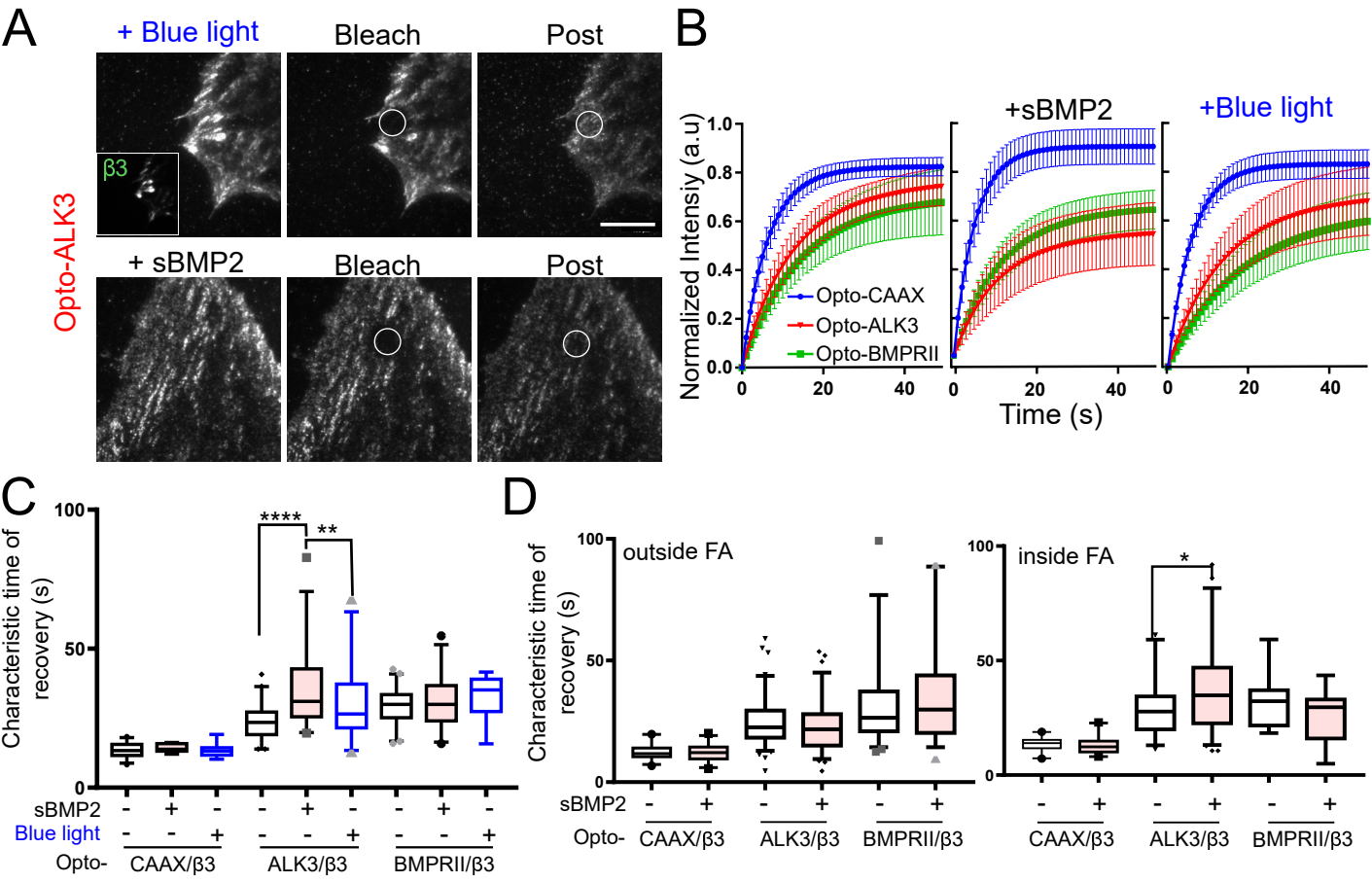

Figure 6. Guevara-Garcia *et al.*

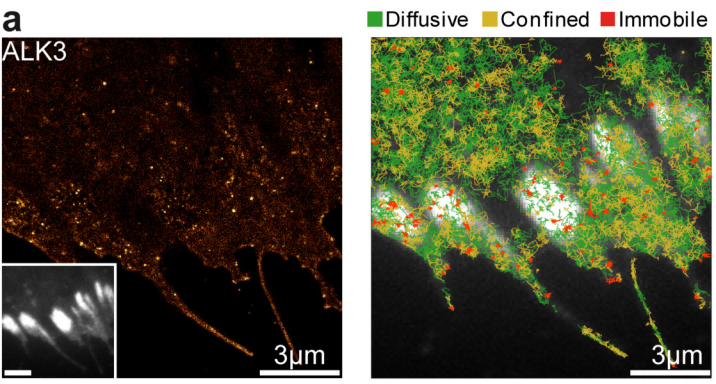


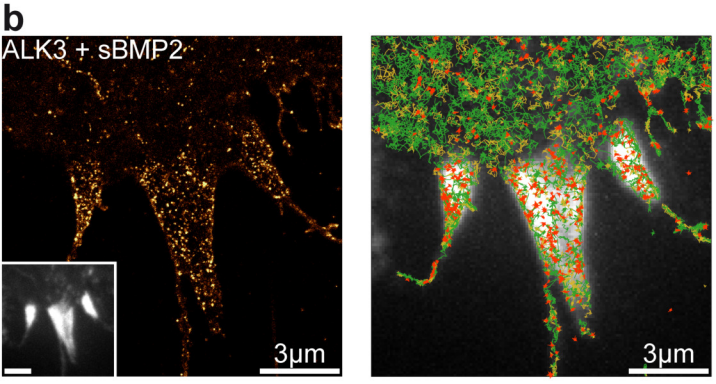


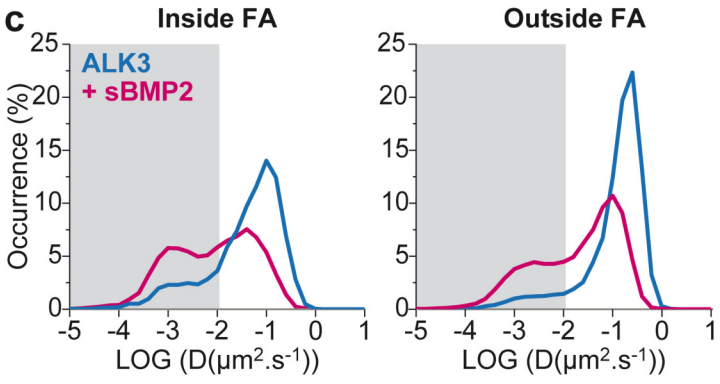


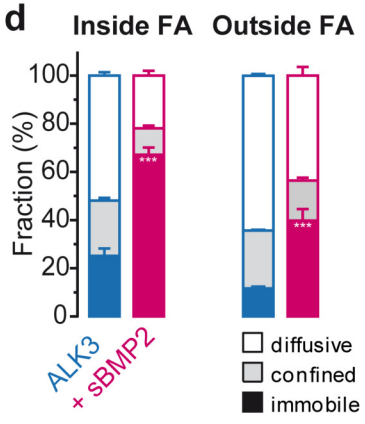


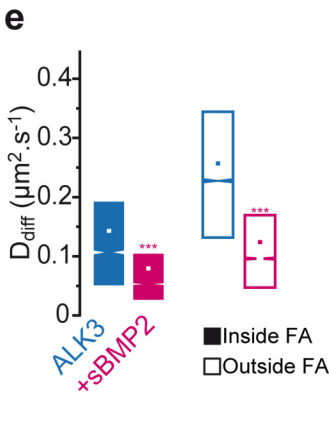


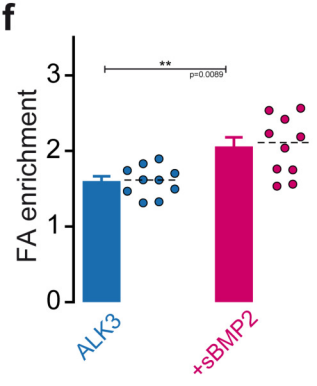

# Figure 7. Guevara-Garcia *et al.*

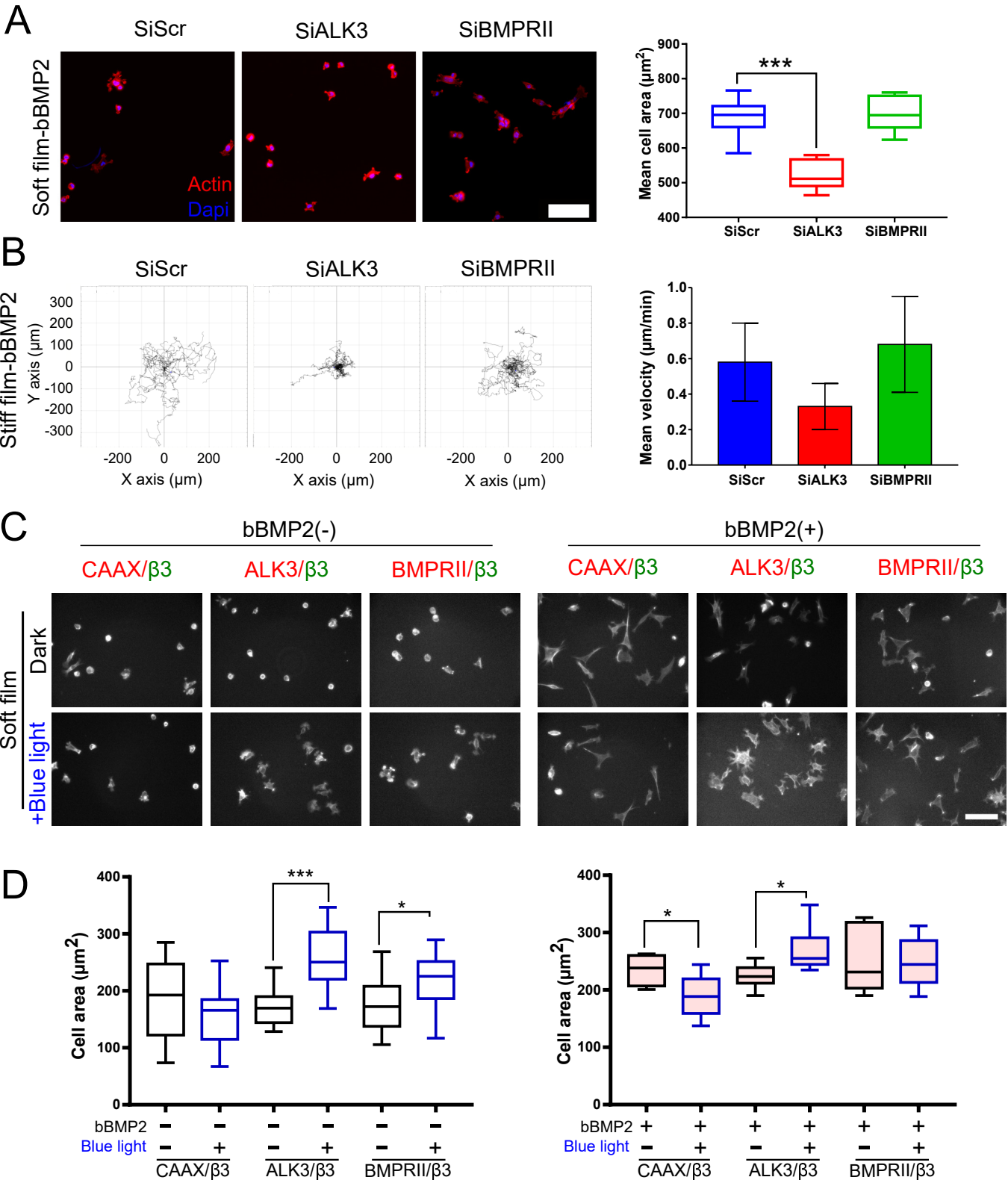

Figure 8. Guevara-Garcia *et al.*

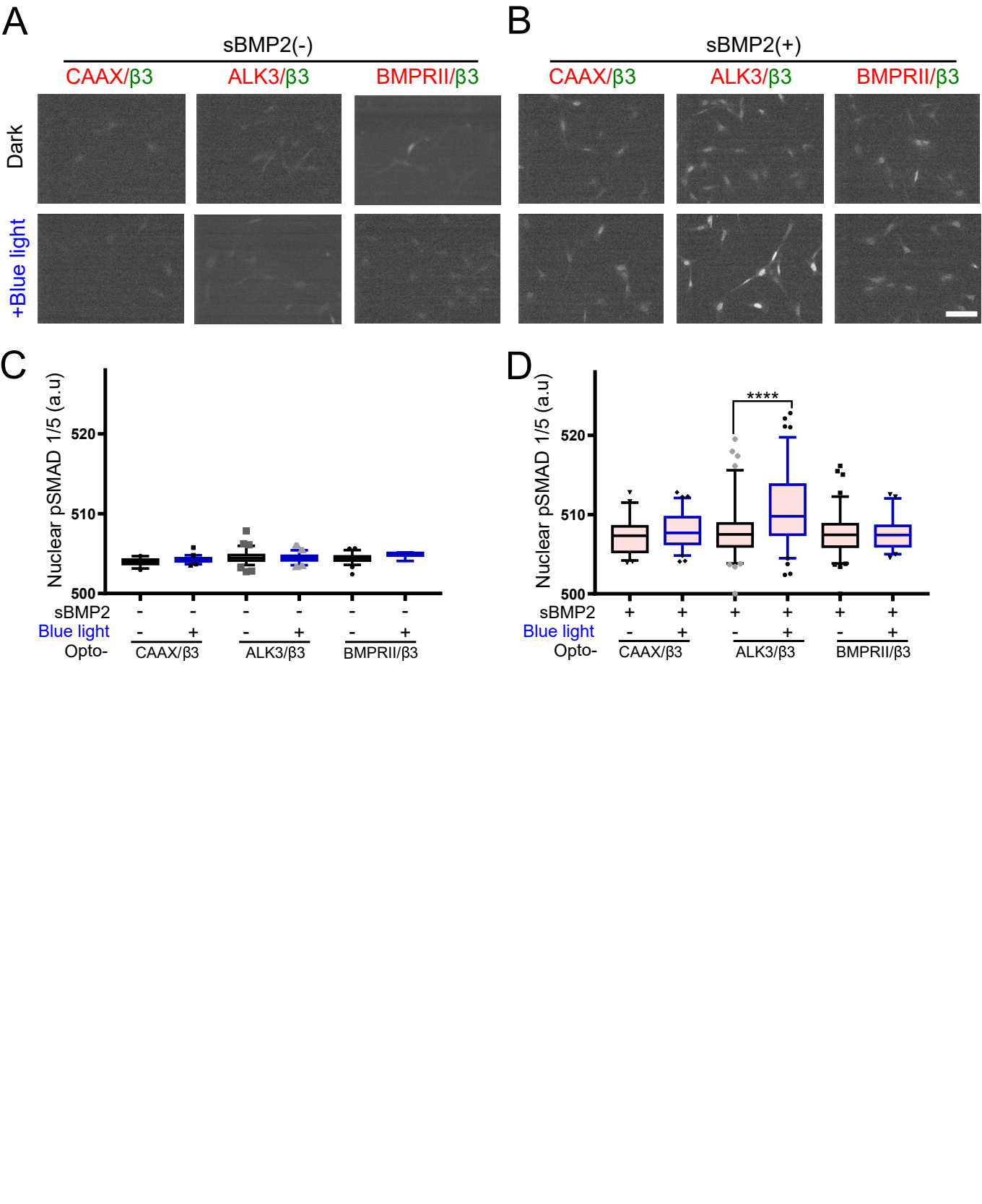

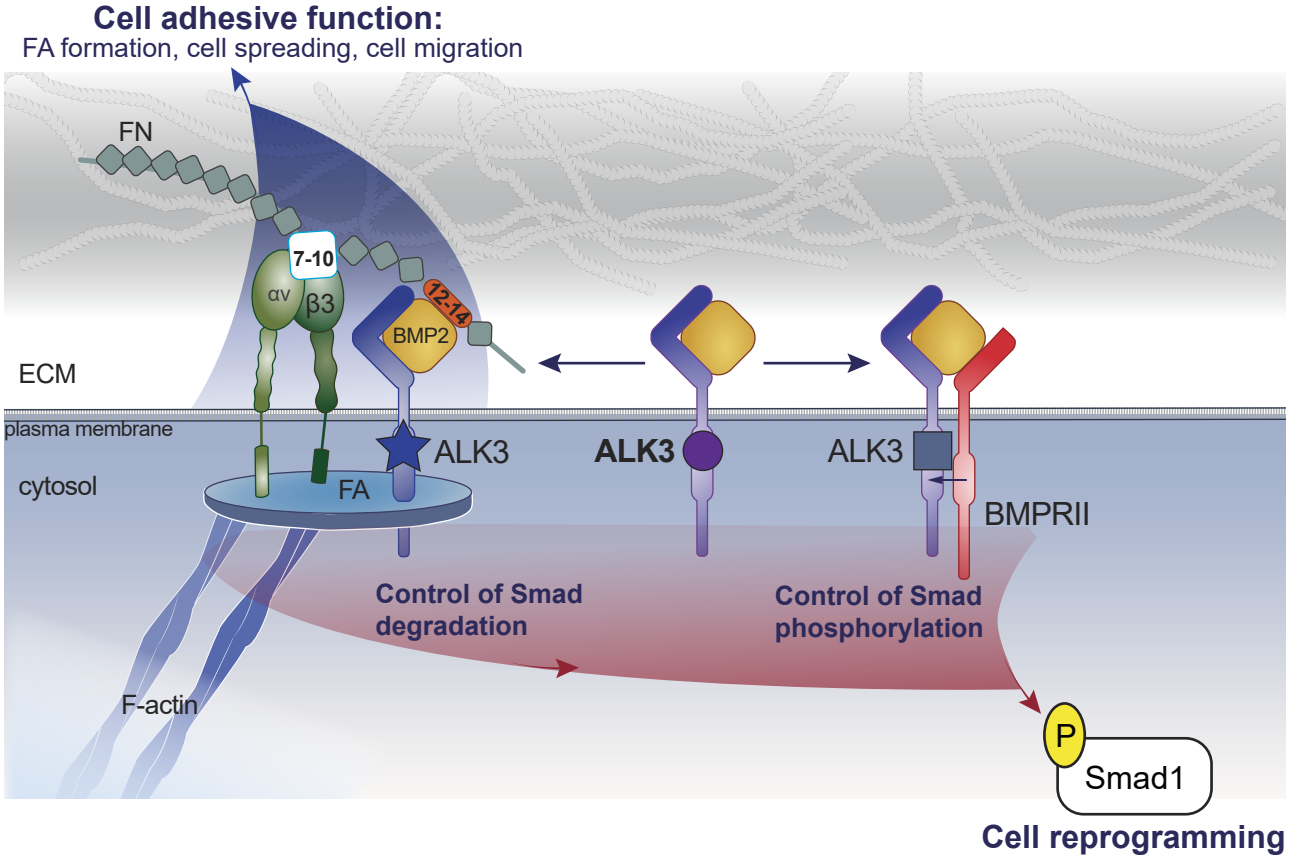
Cell adhesive function:
FA formation, cell spreading, cell migration
FN
7-10
αv
β3
12-14
BMP2
ECM
plasma membrane
cytosol
FA
ALK3
ALK3
ALK3
BMPRII
Control of Smad degradation
Control of Smad phosphorylation
F-actin
P
Smad1
Cell reprogramming

# Figure S1. Guevara-Garcia *et al.*

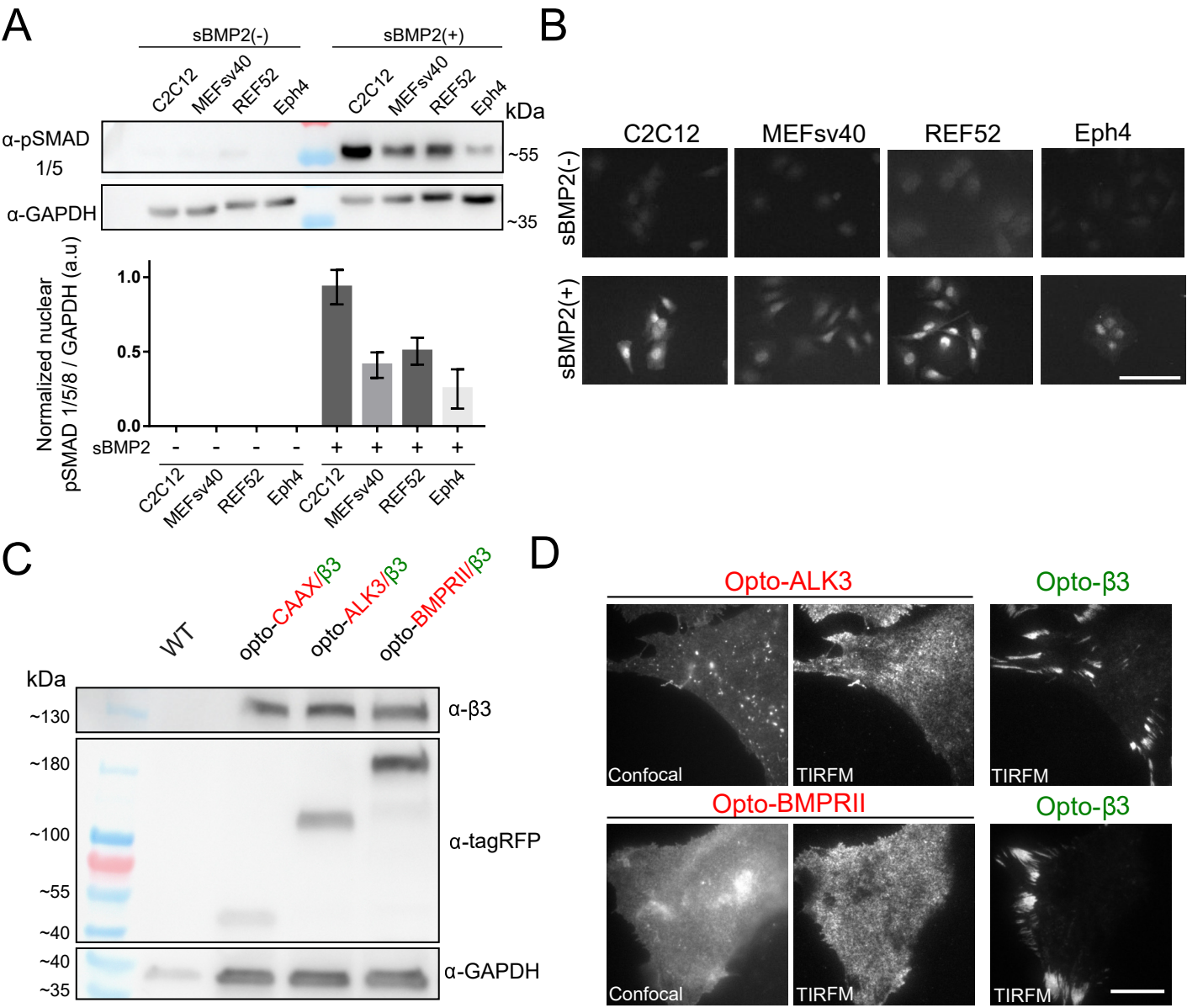

# Figure S2. Guevara-Garcia *et al.*

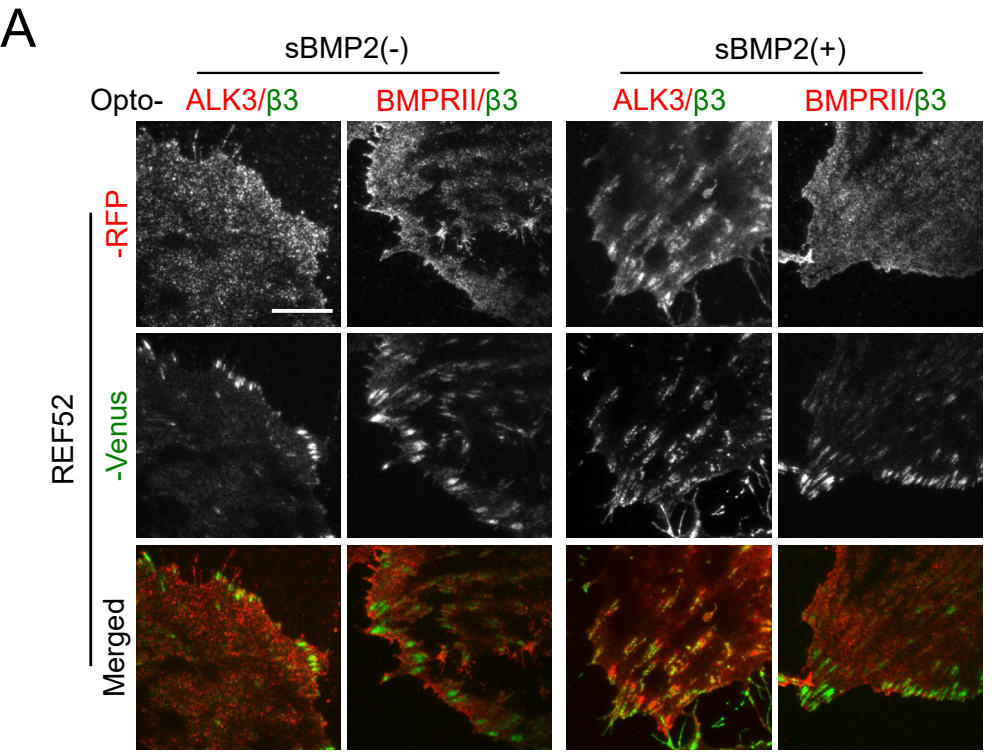


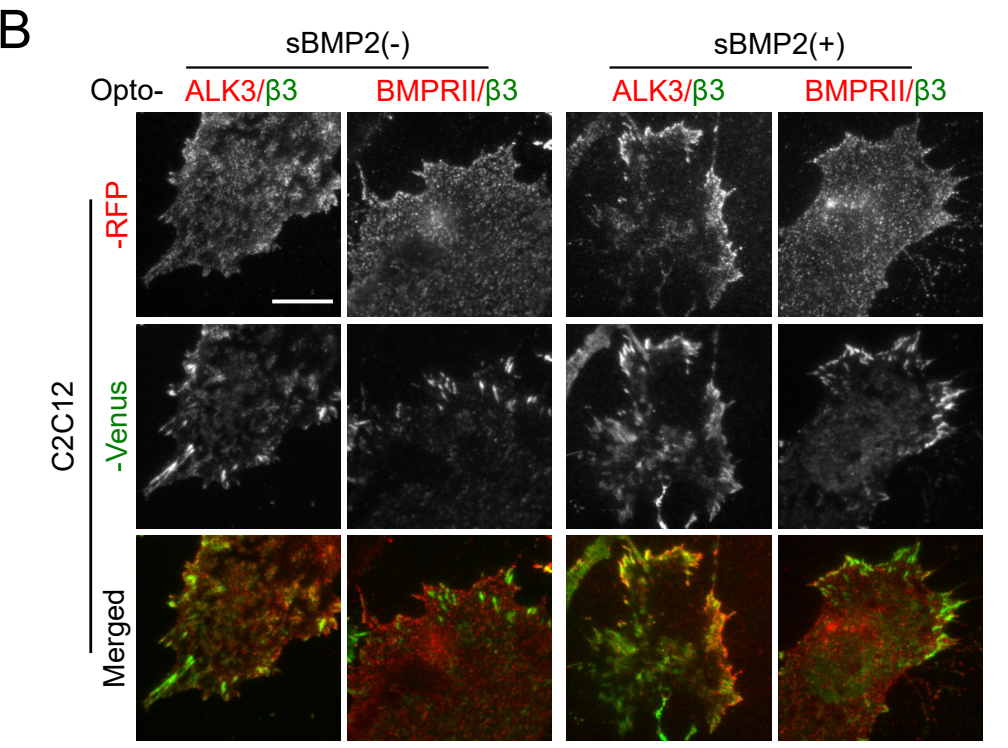


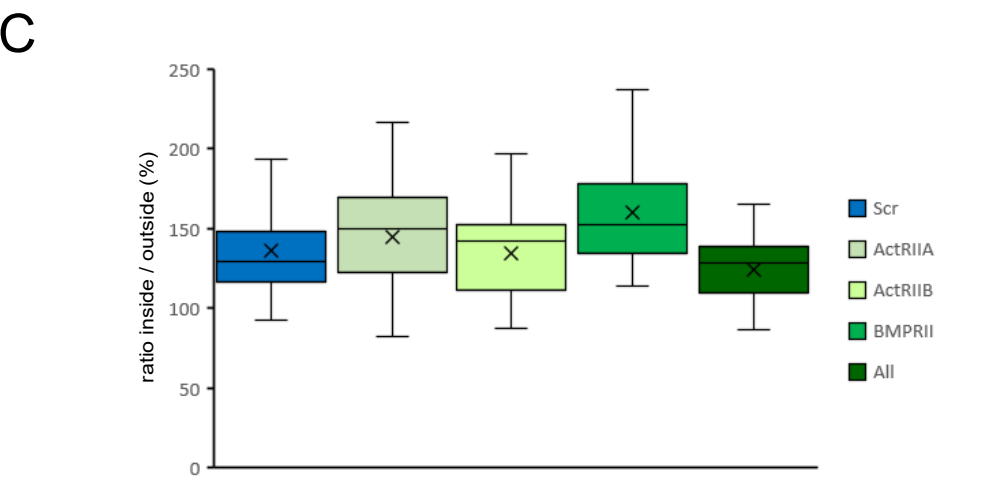

Figure S3 Guevara-Garcia et al.

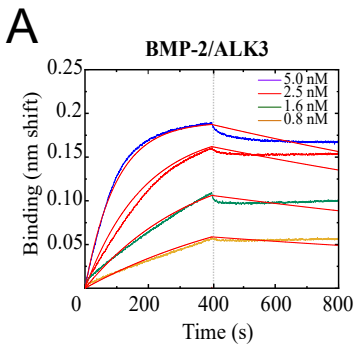


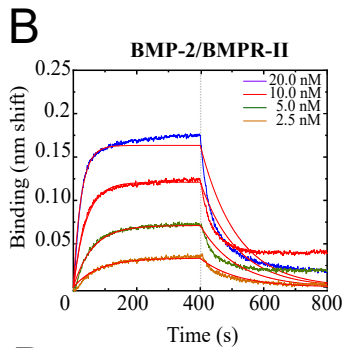


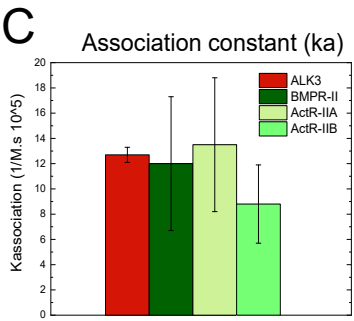


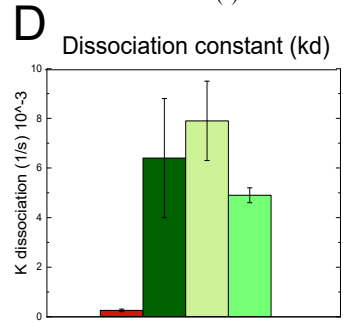


E

| BMP-R | ALK3 | BMPR-II | ACTR-IIA | ACTR-IIB |
|---|---|---|---|---|
| BMP-2 | 0.21 ± 0.03 | 5.4 ± 0.8 | 6.08 ± 1.2 | 6.3 ± 3.4 |

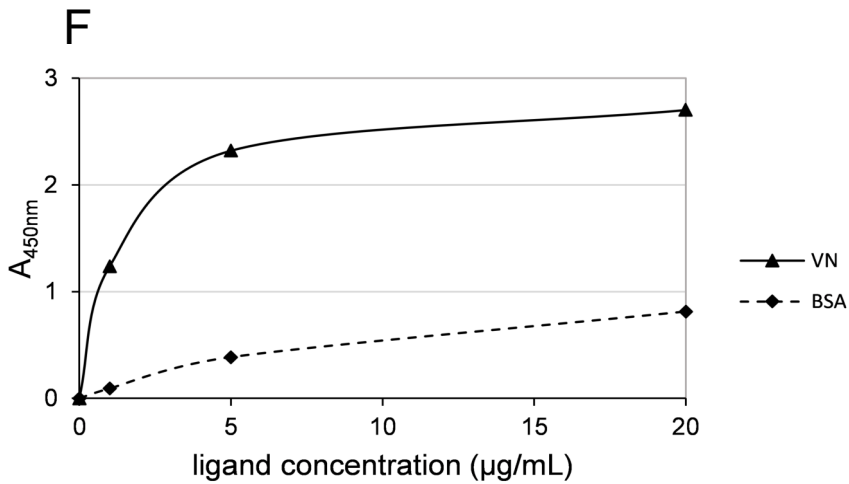

Figure S4. Guevara-Garcia *et al.*

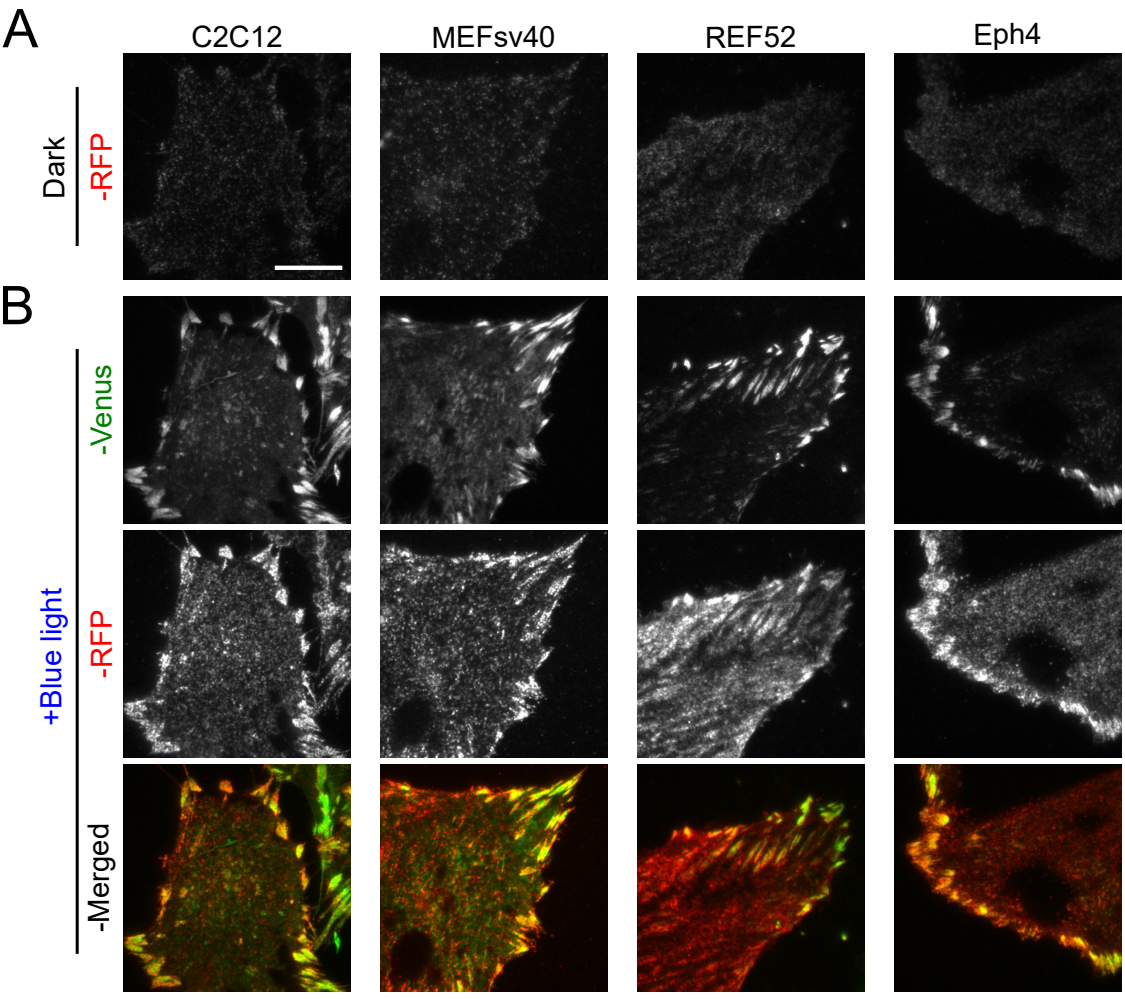


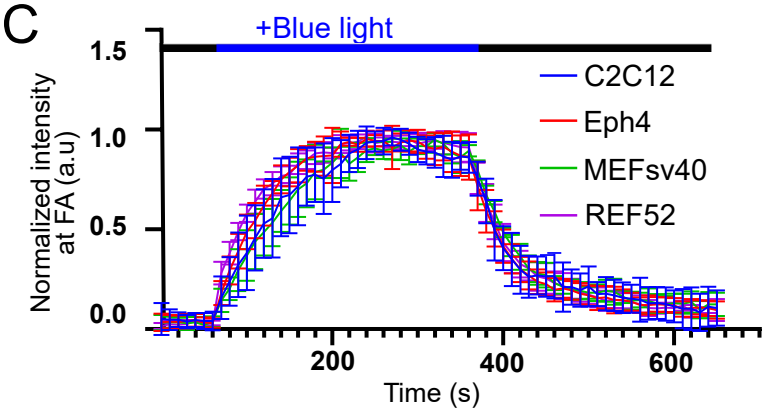

# Figure S5. Guevara-Garcia et al.

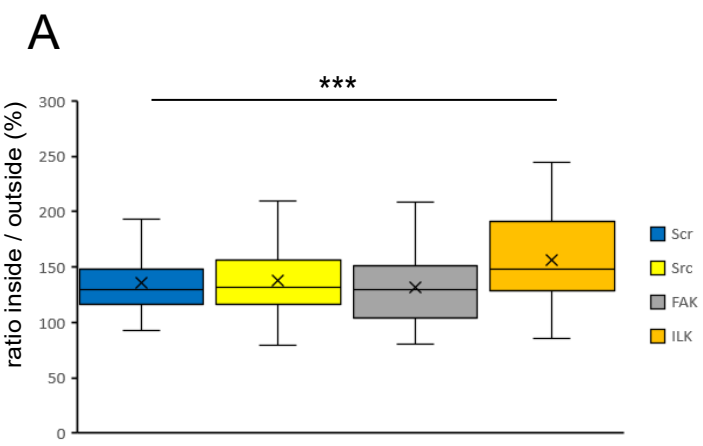


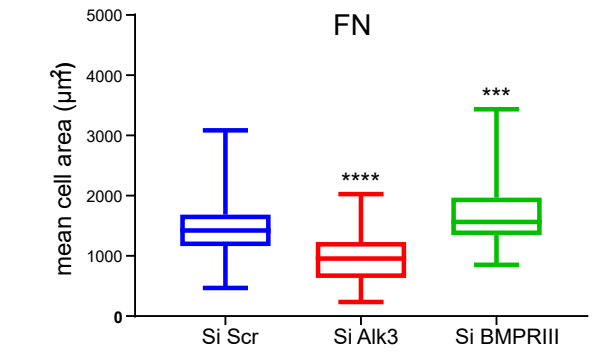


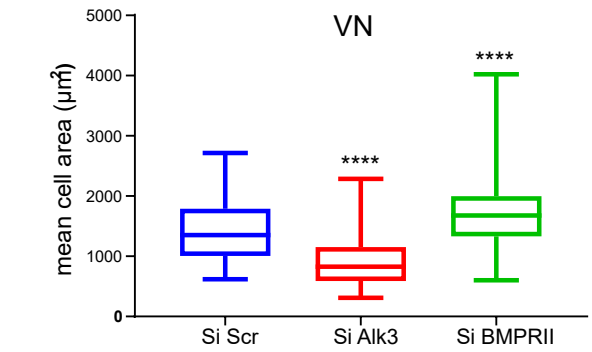


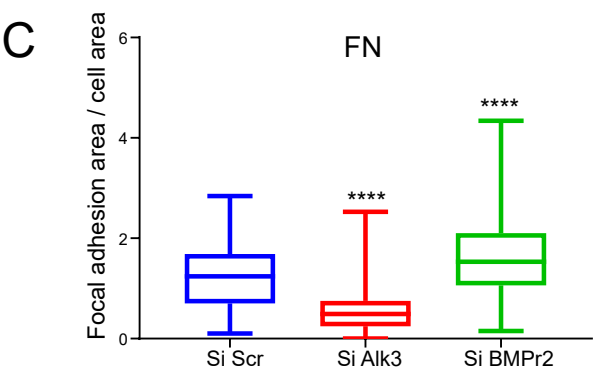


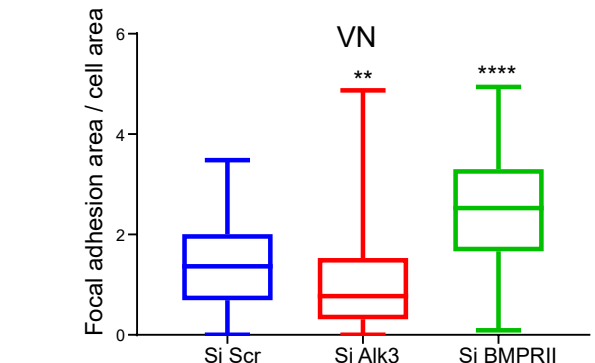


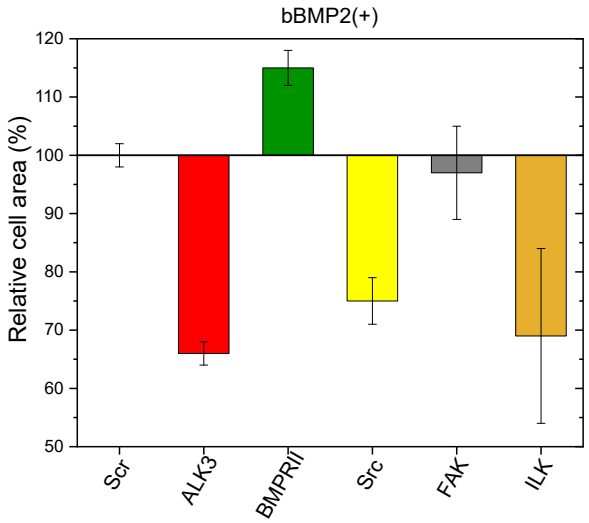


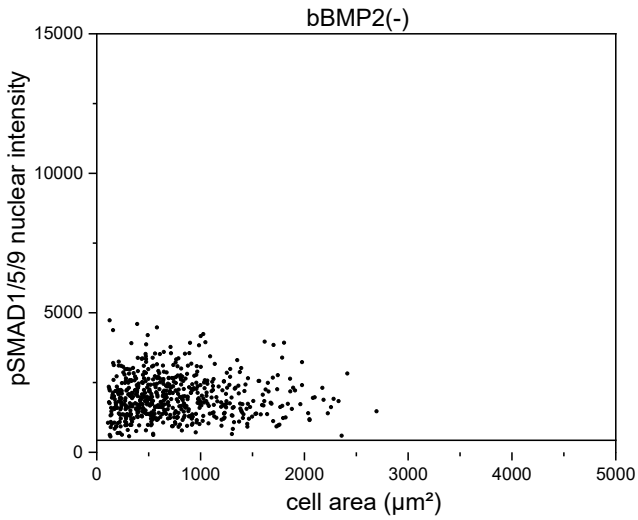


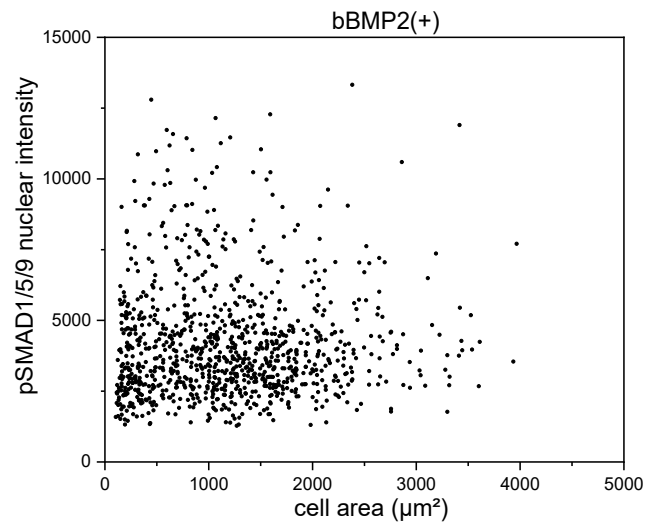


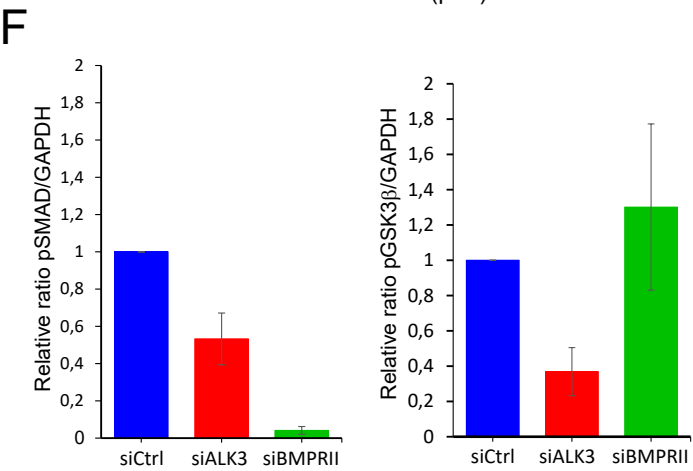

| Name | Sequence | Target |
|---|---|---|
| ALK3 (F) | GGATGCCAAGACCCACTACC | ALK3 |
| ALK3 (ECD) (F) | CTGATTTCATCCCAGTGCC | ALK3 |
| BMPRII (R) | CTGCTCCATATCGACCTCGG | BMPRII |
| BMPRII (ECD) | AGGATGGTCCATGGTAGCCA | BMPRII |
| GFP-N (R) | CCGTCCAGCTCGACCAG | Venus |
| pGFP-C(F) | GATCACATGGTCCTGCTG | Venus |
| RFP (R) | ATCAGCTCTTCGCCCTTAGA | TagRFP |
| pSico (R) | GTACCTAGTGGAACCGGAAC | pSico |
| mPGK (F) | CATTCTGCACGCTTCAAAAG | mPGK |

Supplementary Table 1

| Gene | ID | Animal | Sequence 1 | Sequence 2 |
|---|---|---|---|---|
| Itgb3 | 16416 | mouse | GATTGCCCTTCGACTACGGC | GTCCACGGGGTAATCCTCCA |
| BMPRII | 121168 | mouse | GATCCTGGGCCATCAAAGCC | TGCCATCTTGTGTTGACTCACCT |
| ALK3 | 12166 | mouse | AGGATTCACCGAAAGCCCAG | ATCACGGTTGTAACGACCCC |
| BMPRII | 659 | human | TGGCAGCAGTATACAGATAGGTG | ATGGTTGTAGCAGTGCCTCC |
| ALK3 | 657 | human | ATCACAGGAGGGATCGTGGA | AGACACAATTGGCCGCAAAC |
| BMPRII | 12456 | mouse | GCCCCCTAGTGCTTCTTAGAC | AGCAGCAACACTAGAAGACAG |
| ALK3 | 81507 | rat | GTTTCTCGGGACCCCGATTT | CGGCCACCTTGATTACTGGT |
| BMPRII | 140590 | rat | TGCATTGTAATCCGGGCAGG | AGCCGTTCTTGATTCTGGGA |
| Itgb3 | 29302 | rat | ACCGAAAATGTCGTCAGCCT | GAAGCTCACCGTGTCTCCAA |
| GAPDH | | rat | CAACTCCCTCAAGATTGTCAGCAA | GGCATGGACTGTGGTTCATGA |
| HPRT | | rat | CTCATGGACTGATTATGGACAGGAC | GCAGGTCAGCAAAGAACTTATAGCC |
| TBP | | rat | TGGGATTGTACCACAGCTCC | CTCATGATGACTGCAGCAAACC |
| Rpl13a | | rat | GGATCCCCTCCACCCTATGACA | CTGGTACTTCCACCCGACCTC |
| ATP50 | 28080 | mouse | CAAGCGCACCGTCAAAGTG | GCACCGTCTTTAACTCAGAGAG |
| TBP | | mouse | ACAGCCTTCCACCTTATGCT | GATTGCTCTACTGAGGCTGC |

Supplementary Table 2